

THESIS

A TROPICAL RADIATION AND CLOUD SYSTEM FEEDBACK MODULATED BY SEA  
SURFACE TEMPERATURE

Submitted by

Matthew R. Igel

Department of Atmospheric Science

In partial fulfillment of the requirements

for the Degree of Master of Science

Colorado State University

Fort Collins, Colorado

Fall 2011

Master's Committee:

Advisor: Graeme Stephens

Susan van den Heever

Richard Eykholt

Copyright by Matthew R. Igel 2011

All Rights Reserved

## ABSTRACT

### A TROPICAL RADIATION AND CLOUD SYSTEM FEEDBACK MODULATED BY SEA SURFACE TEMPERATURE

A large domain, high resolution cloud system resolving model set up in the tropics over fixed sea surface temperatures (SST) of 298 K and 302 K and run to radiative convective equilibrium has been analyzed with the focus on well equilibrated, domain mean results. The Regional Atmospheric Modeling System (RAMS) is used. The modeled convection organizes into disturbed, convective and undisturbed, subsidence regions. The mean profiles of state variables such as temperature, relative humidity (RH), and convective mass flux are analyzed and found to depend on SST in both predictable and unpredictable ways. The characteristics of rain depend on SST such that higher surface temperatures produce greater variability in intensity and lesser frequency. Next, the large-scale mean state is used to understand the convective system-scale setup. A focus is on the controls in the undisturbed regions of the disturbed region, deep convective anvil detrainment. Upper tropospheric radiation, through diabatic convergence, is used as a paradigm to understand the height at which detrainment occurs. The dependence of upper tropospheric radiation on RH is derived explicitly for the first time. From this new equation, temperature and RH are found to control anvil detrainment. The addition of RH as an anvil detrainment control explains why the

model leads to an understanding of cooler anvils with higher SST – a positive climate feedback on the system. Other anvil feedbacks exhibited by the model are similar to those proposed in the Iris and Thermostat hypotheses. The convective system components are shown to enhance one another such that the overall system dependence on SST is nonlinear. To understand the circulation system, a heat engine analogue is made that shows the warmer state is able to more efficiently circulate or move heat. Finally, observational evidence from Cloudsat and CALIPSO shows that some of the modeled results are also apparent in nature.

## ACKNOWLEDGEMENTS

The author would like to thank Dr. Graeme Stephens for his advisorship of his work and the opportunities provided thereby. He would also like to thank Dr. Susan van den Heever for her considerable help and guidance during Graeme's attendance to his new duties outside CSU. He would like to thank his remaining committee member for being so obliging. Thanks are due to Adele Igel for her help with the math found in Chapter V. Finally, the author acknowledges the help, both on this project and otherwise, of his various officemates and colleagues here at CSU.

## DEDICATION

I would like to dedicate this work to my parents who instilled in me a curiosity, without which, this work would not have been possible.

## TABLE OF CONTENTS

Abstract.....	ii
Acknowledgements.....	iv
Dedication.....	v
Table of Contents.....	vi
I: Introduction.....	1
II: Background.....	4
Radiation and the Upper Troposphere.....	4
1. The Fixed Anvil Temperature Hypothesis.....	5
2. The Thermostat Hypothesis.....	7
3. The Adaptive Iris Hypothesis.....	8
Model Description.....	9
Experimental Setup.....	11
Radiative Convective Equilibrium.....	13
Experiment Lineage.....	14
Cloudsat and CALIPSO.....	16
III: The Large-Scale, Equilibrated Atmosphere.....	18
Disturbed and Undisturbed Regions.....	18
Domain Averages.....	21
Water Budget.....	25
Precipitation.....	30
IV: The Potential Effects of Enumerated Changes on Anvils.....	35
V: The TUT Radiation Dependence on RH.....	38
Sensitivity.....	42
VI: Simulated UT Radiative Processes.....	46
VII: Model Subsidence Regions.....	51

VIII: Cloud Top Changes.....	56
IX: Synthesis.....	60
Entropy.....	64
Precipitation.....	65
X: Observational Evidence.....	67
XI: Summary and Conclusions.....	71
Works Cited.....	74

## I: INTRODUCTION

This study seeks to elucidate the nature of atmospheric responses to increases in sea surface temperatures through the use of a simple, intuitive, highly idealized framework. In much the same way that Hooke's laws assume a perfect relationship between a mass and a spring which in reality may exist in a rather imperfect physical system in order to find a first order analytical solution, the experiment undertaken here assumes a perfect relationship between surface temperature (SST) and the atmosphere. The model results that comprise this experiment are taken to provide a similar, first order solution of atmospheric responses to different surface temperatures. The obvious extrapolation is to generalize these results to the warmer surface temperature predicted under global warming. Whether or not that is a logical step can be argued, but even absent this mental leap, the examination of the response of the atmosphere in general to surface temperature is a scientifically important endeavor as it allows for the assignment of undeniable cause and effect: effect – increasing total rain; cause – increasing surface temperature. In a system as complex as Earth's atmosphere, changes to atmospheric observables are rarely easily assigned a cause; the atmosphere is after all, compared to our ability to measure its overall state, huge. Therefore, it is the goal of this study to forgo the ambiguity of larger, more complex modeling and true, Earth system measurement experiments by utilizing a simple framework to answer a simple question with not-so-simple implications.

The previous arguments, though, do little to frame the importance of the experiment conducted here. It can be assumed a priori that SST will have an effect on certain atmospheric variables – surface temperature, for instance, will most certainly increase with SST due to energy conservation. However, it is impossible to know the response of relative humidity (RH) to changes in SST without modeling it even given some other, first-order *a priori* results because of the potentially non-constant system-wide controls on RH. Therefore the goal in conducting such an idealized modeling experiment is to ascertain the responses that cannot be assumed.

This experiment will come to imply a complex, mutual interaction between tropical upper tropospheric clouds, RH, radiation to space, and the convective system circulation all modulated by SST. The importance of such results lies in the impact of the tropical convective system. It covers a large region of the planet and is crucial to the global climate system. Local aspects, such as rain amount and rate, are integral to the livelihoods of those who live in the tropics. The new results are realized with a model that spans a variety of scales relevant to both cloud systems and the tropical climate.

The work will proceed as follows. A broad overview will be completed in Chapter II that will focus on several key topics the problem of how the atmosphere might respond to surface temperature changes. The reader should take note of how the enumerated cloud anvil-climate feedbacks in Chapter II all stand alone as this work will attempt to integrate them to form a more complete picture for, to the best of the author's knowledge, the first time. Chapter III will provide the reader with a sense for the way in which the atmosphere appears grossly to depend on SST. From this point,

some of the smaller scale features of the atmosphere may be understood physically before they are examined quantitatively. Chapters V and VI will deal with radiation from the tropical upper troposphere in regions without clouds and how it affects the regions with clouds. The next two chapters complete the convective system-scale circulation. Then the preceding chapters will be examined through a single lens to assess how the components work together and how they may be used to say something about one of weather's most impactful pieces: rain. Finally, Chapter X will backup at least one component of the model dependence on SST with real-world observations.

## II: BACKGROUND

This chapter will seek to put in place the foundation for building the complex feedback that is being proposed. It will focus on: surveying previously researched cloud-radiation feedbacks, understanding the model used to simulate cloud systems, laying out the experimental setup, and understanding the formulations that will help to test the model results.

### *Radiation and the Upper Troposphere*

The tropical upper troposphere (TUT) is an unusual place in the atmosphere. It sees the coldest temperatures anywhere in the global troposphere, interacts with the stratosphere atypically, tops out high (in excess of 15km) (Highwood and Hoskins, 1998). It is also an important component of the climate system as it helps to modulate the radiation leaving the troposphere over half the globe (30°S – 30°N definition of tropics). The radiation emanating from the TUT is greatly affected by the properties of cloudiness there (Stephens *et al*, 1990a). To the best of our understanding, TUT clouds are primarily the result of either concomitant or past convection (Jensen *et al*, 1996). Deep convection lofts moisture with its strong updraft cores into the TUT where it is forced to spread laterally through mechanisms to be discussed. It is the mutual regulation, feedback, of TUT radiation and clouds that will be the primary concern here. A variety of feedback mechanism relating TUT clouds and their effects on radiation

have been proposed recently. Among them are the Fixed Anvil Temperature Hypothesis (Hartmann, 2001), the Thermostat Hypothesis (Ramanathan and Collins, 1991), and the Iris Hypothesis (Lindzen *et al*, 2001).

### *1. The Fixed Anvil Temperature Hypothesis*

The Fixed Anvil Temperature Hypothesis (FAT) was proposed as a constraint on the temperature level at which deep convective clouds would detrain their water mass into horizontally spreading anvils by Hartmann in 2001. The basic premise is that detrainment is controlled by processes which are themselves strong functions of temperature. In a global warming scenario, it was supposed, TUT detrainment temperature would be unaffected. Since the longwave radiation (LW) emitted by cloud tops is taken to be a function of temperature only through the Stefan Boltzmann Law, outgoing longwave radiation (OLR) above clouds would remain unchanged.

The basic physics behind the FAT are well reasoned. According to Zelinka and Hartmann (2010), the rate at which water vapor (WV) can effectively radiate LW falls off sharply below some minimum threshold of WV. If that is taken to be true, then one could find a temperature through the Clausius-Claperyon (CC) relation at which the atmosphere might be likely to hold less than that threshold. This temperature would be a constant throughout the TUT regardless of the local environment (SST, column convective state, etc.).

But how does water vapor LW emission control cloud detrainment? The air with WV mass greater than the threshold will lose energy, *id est* it will cool, more than the air above it through emission to space with less water vapor and less LW emission.

Creating a mass divergence, the moister air will subside away from the drier air above as it cools. Through continuity arguments, it can be seen that clouds must detrain at this level.

Kuang and Hartmann (2007) state that in the TUT, a balance must exist between clear-sky radiative cooling and warming due to subsidence. This can be stated mathematically as:

$$\omega \frac{d\theta}{dp} = \frac{\theta}{T} Q \text{ (Eq1)}$$

where  $\omega$  is the pressure velocity,  $\theta$  is potential temperature,  $T$  is physical temperature, and  $Q$  is clear sky cooling. Because mass is being neither created nor destroyed in the atmosphere, the continuity equation may be used in the following form:

$$\frac{du}{dx} + \frac{dv}{dy} + \frac{d\omega}{dp} = 0 \text{ (Eq2)}.$$

$u$  and  $v$  are the horizontal components of the wind. Upon rearranging:

$$-\nabla \cdot U = \frac{d\omega}{dp} \text{ (Eq3)}.$$

$U$  is the horizontal wind. If Eq1 is rearranged to diagnose  $\omega$ , Eq3 may be used to diagnose the horizontal convergence ( $-\nabla \cdot U$ ), in this case, termed diabatic convergence (DC). This clear-sky convergence dictates the level at which TUT detrainment occurs and has a sharp peak where Hartmann predicted. This would seem to be a strong physical constraint.

There has been a community effort to test this hypothesis with both models and observations. Kuang and Hartmann use a model and find both that the WV concentration drop off in the TUT, not the ozone profile as may be assumed, controls

the detrainment level and that the anvils detrain at a nearly constant temperature. They find only a 0.5K increase in anvil temperature per 2K of SST increase. This result is in direct contrast to what will be shown here. While the Kuang and Hartmann study has smaller vertical grid spacing in the upper troposphere that this study will employ, it is limited in horizontal domain. Their study uses just over 4,000 planar grid points, extending over an area of 64 km by 64 km whereas this study uses 300,000 (or nearly two orders of magnitude more) with an area of 9600 km by 180 km.

Their study shows that divergence in the TUT is strongly controlled by local TUT temperature. Likewise the normalized cloud fraction appears to be dependent on temperature only. These results will be tested here.

## *2. The Thermostat Hypothesis*

The Thermostat hypothesis was originally proposed in 1991 by Ramanathan and Collins. As the name may suggest, it is a theory that attempts to explain the self-regulation of temperature in the atmosphere. Like the FAT, the crux of the argument relies on TUT clouds – here, primarily as a reflector of incoming shortwave radiation (SW).

Ramanathan and Collins use data collected during a warm phase of the tropical Pacific, an El Nino, and compared it with data taken during an unperturbed period. They found that the reflectivity of cirrus anvils was greater during the warmer SST period. This led them to conclude that SSTs must have some control over cirrus such that a negative feedback existed in which a warmer environment created thicker cirrus and was cooled by more reflective cirrus. The mechanisms for such a feedback are simple ones. As SSTs increase, total column WV has been shown to increase (Stephens,

1990b; Vecchi and Soden, 2007; Held and Soden, 2006). As WV availability increases, the convection is better able to transport vapor from the boundary layer into the upper levels. This greater water flux results in anvils that are physically and/or optically thicker. Since the anvils are more reflective, less SW radiation reaches the surface. So, the warmer state is cooled by the moister convection it induces.

This is an elegant theory given that, in principle, the atmospheric system must be made up of a variety of negative feedbacks or else climate would not be stable. The radiation into the system from the sun provides a strong spherical boundary condition that should help to stabilize the system to small perturbations, but other internal negative feedbacks must also be at play given that a variety of positive feedbacks have been found in the climate. However, there has been some evidence to suggest such a feedback does not exist (Fu *et al*, 1992).

Nothing is made, however, of the LW effect these anvils have on emission from the surface and from WV. The Thermostat Hypothesis can only exist if the effects on LW are negligible compared to SW effects; this is something to be discussed here.

### *3. The Adaptive Iris Hypothesis*

In 2001, Lindzen *et al*. developed an interesting, though much maligned, theory yet again relating TUT anvils and LW radiation escaping to space. In its most basic form, the theory states that as SSTs increase, anvil areal extent decreases. Although the physical existence of the hypothesis has been called into question (Del Genio and Kovari 2002, Lin *et al* 2004, among others) (especially the use of cloud-weighted SST), it nonetheless deserves some investigation for the same reasons as the Thermostat Hypothesis, and if somehow proven, would be a boon to the cloud-climate-interaction

community. Su *et al.* (2008) show that ice water path actually increases with SST which would seem to be in conflict with the Iris.

Lindzen *et al.* (2001) spend some time discussing how such a feedback might work. For brevity, I will only mention here that the primary mechanism is an increase in PE, precipitation efficiency. PE is a measure of the cloud-scale moisture fluxes into the storm base relative to the precipitation leaving it. A higher PE indicates more rain per unit positive, inward moisture flux from the low-level entrainment of warm, moist boundary layer air and negative flux of anvil ice as it evaporates at cloud edge. Thus, for a given precipitation rate, an increase in PE would require less moisture into the storm from the lower levels or more anvil detrainment. Increasing SSTs is unlikely to decrease surface moisture fluxes significantly so if PE increases sufficiently, anvil detrainment is likely to decrease. PE is only one possible explanation for the adaptive iris. It will be shown here that another mechanism may be at work.

### *Model Description*

A General circulation model (GCM) is the standard tool used to assess the implications of changes in surface temperatures; here, a different approach is taken. A mesoscale model on a large domain is used in an attempt to simulate a large enough area to give credence to the results while still retaining the benefits of such a model given the coarse grid size required by computational constraints. Among the benefits of this approach is the explicit representation of cloud systems hence the nomenclature, cloud system resolving model (CSRМ), used in the community and throughout this document.

The mesoscale CSRM used here is the Regional Atmospheric Modeling System, or RAMS. It was originally developed here at Colorado State University. The name is a play on the school mascot. It was originally written piecemeal and unified by the Pielke Sr. and Cotton research groups (Pielke, 1992) and has been continuously updated and improved thanks to the efforts of numerous other research groups here at CSU and afield.

RAMS is a compressible, non-hydrostatic model of the Navier-Stokes equations. The Navier-Stokes equations form a set of partial differential equations which, when solved simultaneously, predict the future state of a fluid in question. In RAMS, that fluid is the atmosphere, a continuous fluid too large to be solved analytically. Therefore, RAMS makes use of a variety of approximations and discretizations.

Variables are arranged on an Arakawa-C grid. In a 3-dimensional model, this means that the three components of the wind are predicted on the six surfaces of a box surrounding a center point on which scalar quantities are predicted. Adjacent scalar points share a box side, and therefore, a wind value. Such “staggering” allows for convenient computation of equations relevant to atmospheric motions.

Other important parameterizations include the surface and turbulent formulations. Sensible and latent heating, as well as the partitioning between them, were parameterized using the Land Ecosystem-Atmosphere Feedback-2 (LEAF-2) (Walko et al. 2000). Turbulence is simulated using a K closure scheme of Smagorinsky (1963) with the stability modification of Lilly (1962) and Hill (1974).

Cloud microphysics is represented in this implementation of RAMS by a single moment scheme (Walko et al 1995). Cloud droplets are represented by a bimodal

distribution with modal diameter bins from 1-40 $\mu\text{m}$  and 40-80 $\mu\text{m}$ . Raindrops are unimodal. Ice species include small and large homogeneously and heterogeneously nucleated crystals, aggregates, hail, and graupel. Collection is stochastic. Utilizing a shape parameter of 2, particle spectra distributions are represented with a generalized gamma function. While a double moment scheme may have been preferable for a detailed examination of clouds, the mean states that are to be detailed below would seem to be adequately represented with the single moment scheme required by computational constraints.

The SW and LW fluxes are calculated using a two-stream scheme implemented by Harrington (1997). Two-stream methods allow for radiation to flow in opposite directions normally along the zenith and azimuth and allow for multiple scattering (an inherently important process for SW-cloud interactions). They are computationally tractable though fall physically short of the complete radiative transfer equations. It should be noted that the radiative arguments to come are limited by the assumptions of the two-stream model.

### *Experimental Setup*

As was discussed in the introduction, the model runs to be analyzed here were set up such that one state variable was controlled and changed – SST. SST was fixed in time for simplicity and to get a better understanding of its controls on the atmospheric system than if it had been able to respond to the atmosphere. A fixed SST is, perhaps, unrealistic, but rather than arbitrarily fixed, it may be better to imagine the sea surface as having a very long response time or an extremely deep mixed layer. While three

SSTs simulations, 298K, 300K, and 302K, were run, only the coolest (referred to as SST298) and warmest (SST302) are to be analyzed here. The 300K run was the control and led initial credence to the results. Including the 300K run, though, would provide little additional information as many of the domain mean quantities to be assessed below change monotonically with SST. To be fair, some transitions are not monotonic. It is the author's opinion that while the magnitudes of the trends to be discussed may change with the inclusion of the control run, the overall results would not change but would simply be more muddled. Including only SST298 and SST302, also better fits with the idealized nature of this work. Full details of these runs, including the 300K control simulation, have been described in detail elsewhere and the reader is referred to these works (Stephens *et al*, 2008a; Posselt *et al*, 2008)

The runs were each initialized with a sounding from the TOGA-COARE (The Coupled Ocean Atmosphere Response Experiment of the Tropical Ocean and Global Atmosphere Programme) field campaign conducted in the tropical Pacific. The initialization included a quiescent flow in the horizontal and vertical and small random perturbations to potential temperature to eventually induce motions. The model has no diurnal cycle as solar insolation is fixed (because of the RCE framework to be discussed next) at nearly the tropical yearly average of  $447.2 \text{ W m}^{-2}$ , which allows for a convenient solar zenith angle of  $50^\circ$ . A gravity wave absorber was included in the top 4 layers. Periodic lateral boundary conditions were used. Since this study approximates the tropics, the coriolis parameter was set to zero everywhere.

This implementation of RAMS is three-dimensional. True spatial dimensionality has been shown to be important in accurately simulating observed convective

circulations (Tompkins, 2000). Computational expense, however, can be intractable if the constructed domain is too large. To balance this concern, the model was run in a “canyon” configuration which is long in one horizontal direction and short in another similar to other studies (Tompkins, 2001). The long dimension is 4,000 gridpoints at 2.4km each for a zonal length of 9,600 km; the short is 75 for a meridional of 180 km. The total area is an impressive 1.728 million km<sup>2</sup>. 37 vertical levels are output with lesser spacing, in both physical and pressure spaces, between levels near the surface.

The model was run for 55 days of which the final week will be used for analysis to ensure no contamination from the equilibration period that lasts for about the first month. The equilibration is shown elsewhere and omitted here (see Posselt *et al.*, 2008 or Stephens *et al.*, 2008a for a discussion of the equilibration time). Interestingly, the model domain is so large that simple domain statistics of state variables for each SST run tend to look the same if values at just a single output step or the final week’s are used.

### *Radiative Convective Equilibrium*

Radiative Convective Equilibrium (RCE) is a paradigm originally introduced by Manabe and Strickler in 1964. A way to develop this framework is to imagine a simple model of atmospheric radiative transfer that might split the atmosphere into distinct layers and assume each layer is a black body. The black body assumption would imply that radiation leaving one layer in either the zenith or azimuth direction would be completely absorbed by its neighboring layer. Such a model yields an atmosphere that cools with height at a rate (its lapse rate) of about 13K km<sup>-1</sup> ( $\Gamma_{\text{rad}}$ ), yet Earth’s tropical

lapse rate is observed to be closer to  $6.5\text{K km}^{-1}$  ( $\Gamma_{\text{RCE}}$ ). In order to make the lapse rate of this simple slab model fit better to observations, energy is artificially transported upward until  $\Gamma_{\text{RCE}}$  is reached. The simplest way to transport this energy is through the vertical motion of warm air from below, convection. Convection both redistributes sensible heat as well as releases latent heat. Hence a balance sets up between radiation constantly attempting to steepen the lapse rate to  $\Gamma_{\text{rad}}$  and the convection that is forced vertically to maintain the lapse rate at  $\Gamma_{\text{RCE}}$  or less. RCE has proven a good approximation of the tropical atmosphere.

As such, the model used here is run in an RCE framework. The equilibration time mentioned above is the model moving from its initial state into RCE. But, RCE is another limitation to the arguments presented below. The model is forced with an arbitrarily induced redistribution of energy into some standardized state based on observations (of lapse rate). The energy arguments from model output can only be as strong as the arbitrary *a priori* assumptions that go into the RCE paradigm. That being said, RCE has proven to be a robust framework, and the energy argument issues tend to be ignored.

### *Experiment Lineage*

The RAMS-RCE-fixed SST framework has been used to great effect in a variety of studies. Both two and three-dimensional simulations have been conducted. As was mentioned above, three dimensions are crucial to accurately resolving the complex circulations that set up in the tropics between convective and quiet, subsidence regions. Though 3-D and 2-D models grossly form the same convective and suppressed region

circulation, the scales or circulation are much more accurately simulated in 3 dimensions (Tompkins, 2000).

In 2008, Posselt *et al.* examined these same model runs with the intent of analyzing stable layers and how they related to the trimodal nature of cloud top heights observed tropical convection (Johnson *et al.*, 1999). Posselt *et al.* describe three circulations that form at equilibrium and relate these to the three peaks in cloud top height. Air rises in convective cells, detrains (as above) at cloud top, and spreads horizontally. Due to cooling or continuity, air sinks at some distance away from the cloud top. Subsiding air warms adiabatically (the product of pressure and volume raised to a power dictated by the molecular degrees of freedom is constant for the process). Eventually forcing the air to converge back toward the convecting cell, the warmed air creates a stable layer in the atmosphere that the subsiding air cannot penetrate vertically. The results from Posselt *et al.* suggest that the stable layers depend on the strength of the circulation, through subsidence, not on thermodynamic state transitions as had been suggested before (Mapes and Houze, 1995). The indirect result of these findings is a new way to assess the strength of modeled circulations. Additionally, Posselt *et al.* note that the lowest stable layer, usually associated with the atmospheric boundary layer, is split in these model runs around the boundary layer. The split does not induce an extra circulation.

In 2009, Pakula and Stephens used the System for Atmospheric Modeling Cloud Resolving Model with a sophisticated radiation scheme. They also used a tropical, RCE, though two-dimensional, set up similar to the RAMS setup above. This study sought to understand the effects of the profile of radiation on the RCE equilibrium. Helping to

enhance the stable layers, radiation cools below the relative humidity (RH) gradient induced by the subsidence and warms above it. But, they find that the dynamics are more important in maintaining these stable layers than the RH gradient.

### *Cloudsat and CALIPSO*

Real world observations will be used in this study in addition to the model runs to lend some credence to the model results. Cloudsat and CALIPSO (Cloud Aerosol Lidar and Infrared Pathfinder Satellite Observations) are part of the A-Train of Earth observing satellites. They were launched in 2006 with the combined mission of helping to improve our understanding of clouds in the climate system (Stephens and Vane, 2007). Cloudsat observes clouds and light rain with a 94 GHz radar sensitive to returns of -30dBZ with 500m vertical resolution. CALIPSO utilizes a lidar (the Cloud-Aerosol Lidar with Orthogonal Polarization) at 532nm and a frequency doubled signal at 1064nm with vertical resolution of 30-60m and is sensitive to returns as low as those from optically thin clouds and aerosols. Here, the combination of these sensitivities will be used to look at deep convective tops and detraining anvils in the upper troposphere.

The combined Cloudsat and CALIPSO products include the European Center for Medium-Range Weather Forecasts model of the atmosphere to provide a suite of meteorological variables calculated from other instruments that are not measured by these two satellites. For the requirements of this study, flux-heating rates will be obtained from the ECMWF reanalysis product. The normal flux product uses the radar return from Cloudsat to calculate fluxes (L'Ecuyer *et al*, 2007), but here, the clear sky fluxes will be the main concern. The Cloudsat flux is insufficient for this purpose

because it calculates fluxes based on cloudy retrievals. The clear sky fluxes are calculated using ECMWF data. To examine cloud occurrence in the TUT, the GEOPROF-LIDAR product will provide data. In this product the radar and lidar provide complimentary information to retrieve both optically thick (deep convective towers) and optically thin (detraining cirrus) clouds (Mace *et al*, 2007).

### III: THE LARGE-SCALE, EQUILIBRATED ATMOSPHERE

The most striking dependence of the modeled atmosphere to SST is how the large-scale setup changes. It has been shown elsewhere that scales of convection that form in response to an imposed SST in an RCE model like this are sensitive to the surface conditions. In this chapter, an emphasis will be paid to examining how the atmospheric state changes *en masse*. Enumerating large-scale sensitivities should help to contextualize the smaller-scale changes to be discussed in later chapters.

#### *Disturbed and Undisturbed Regions*

As the circulation discussion above would imply, the modeled atmosphere forms a number of regions of generally rising air and generally subsiding air. The regions of ascent are characterized by cloudiness topping out at a variety of altitudes, precipitation, high RH, and low OLR. The regions of descent generally form boundary layer clouds, may be partially covered by detrained anvil cirrus, rain very lightly, if at all, have low RH, and emit high TOA OLR. The relative areas of these regions have been supposed to be important for climate (Pierrehumbert, 1995). For a good numerical discussion of the aggregation of convective zones see Su *et al.* (2000) and Mapes (1993).

The sensitivity of the scales of convection to SST is manifest in the fixed domain size of this model as an increase in the number of the simulated disturbed/undisturbed

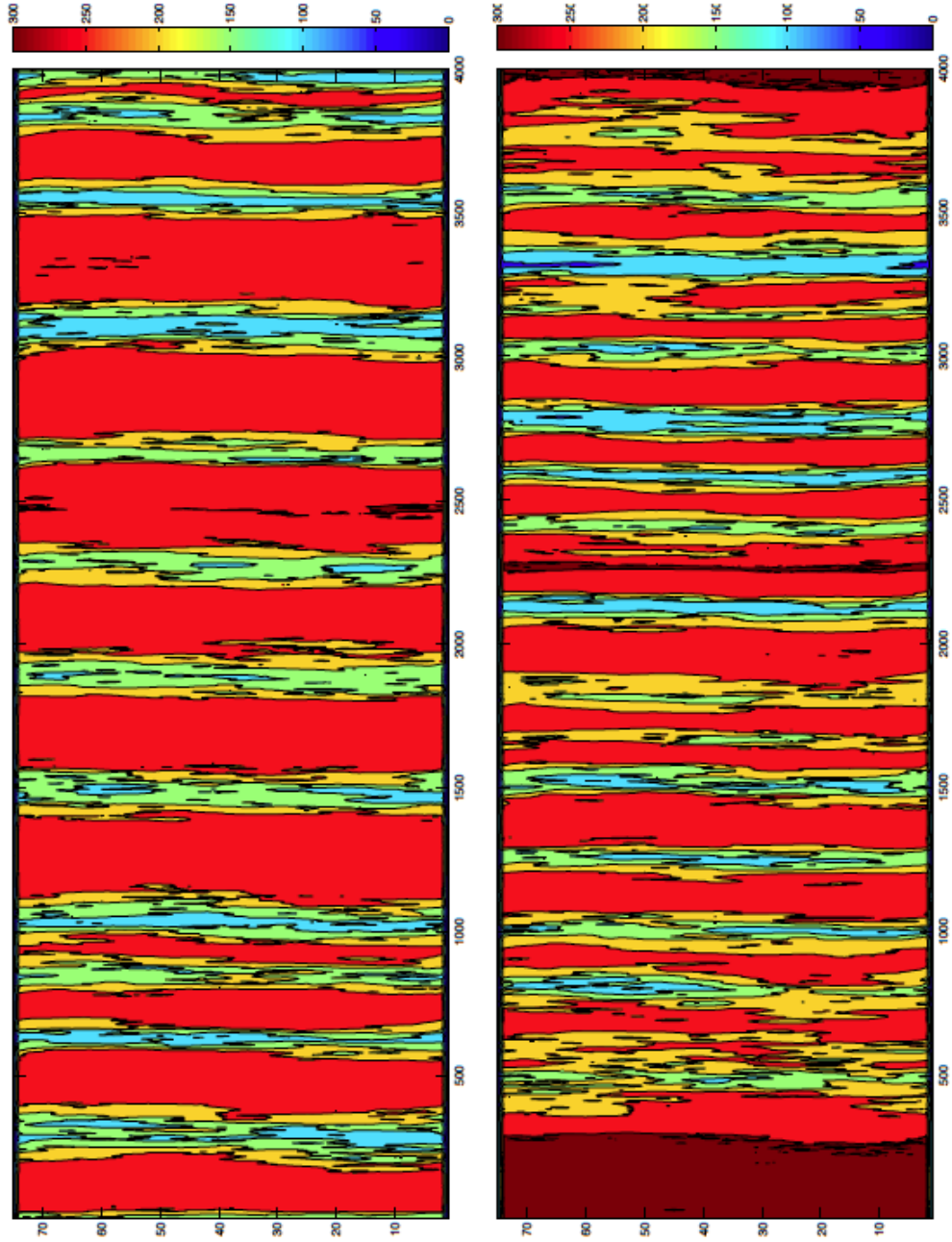
regions. Figure 1 shows time averaged OLR. The disturbed/undisturbed dichotomy (illustrated as high and low OLR, respectively) is obvious in both panels.

The sensitivity to SST in the distance between disturbed regions is also apparent. Figure 1 also shows that SST302 exhibits, even with a temporal average, an increase in the occurrence of both extremely high OLR in undisturbed regions (say,  $>250 \text{ W m}^{-2}$ ) and extremely low OLR in disturbed regions ( $< 80 \text{ W m}^{-2}$ ). Finally, it should be noted that pixels are not square in Figure 1. The meridional direction is stretched relative to the zonal. This is simply done because the zonal direction is so much longer than the meridional and to show some of the structure of the disturbed regions. When pixels are forced to be square, individual cloud structures are seen to be simulated realistically, quasi-circular.

A variety of definitions can be used to define the disturbed regions of the domain for mathematical purposes. Regions can be selected based on: a maximum OLR threshold, column-integrated WV commonly called precipitable water (PW), or a threshold of cloudiness. It is the latter that will often be used here. This filter assesses whether a cloud, defined as a scalar grid point with total condensate at or above  $0.01 \text{ g kg}^{-1}$  mixing ratio (Grabowski and Moncrieff, 2001), exists above 3 km. Applying the filter passes regions with active congestus and deep convection, and blocks regions of low-level clouds unless they are overlain by thick cirrus. Results are insensitive to the filter that is applied due to the overlap of filters and the spatiotemporal averaging. Undisturbed regions are defined as any pixel not classified as disturbed.

**Figure 1.**

Total domain  
OLR from the  
final time  
step. Warm  
colors (high  
OLR) imply  
undisturbed  
regions while  
cool (low  
OLR), imply  
disturbed.  
The size of  
regions can  
be seen to  
shrink with  
SST. Upper  
plot is  
SST298;  
lower plot is  
SST302.



### *Domain Averages*

Perhaps the most robust sensitivities to SST of the simulated atmosphere are the domain averaged state variables. Quantities such as temperature, RH, and PW are so well equilibrated within disturbed and undisturbed regions that their standard deviations over space and time are very small. Understanding how the atmospheric state changes helps to explain some of the later results.

*A priori* we may assume that since SST changes, the profile of temperature must also change (at least near the surface). Indeed near surface air temperature does increase from SST298 to SST302, but the way in which the entire column changes is more interesting. Figure 2 shows the domain mean temperature profiles from the two model runs and the change from SST298 to SST302. The profiles are broadly similar with a few notable differences. The first is the increase in temperature in the lower atmosphere. The second panel shows that the increase is greater in the upper troposphere (9-13 km) than in the lower. This is probably due to change in shape of pseudo-adiabatic temperature profiles with surface temperature, a feature commonly noted in GCM climate experiments (Ye *et al*, 1998; Sherwood *et al*, 2010). The pseudo-adiabats depend weakly, but non-negligibly, on WV content. Since the warmer state has higher PW (shown next), the pseudo-adiabat in SST302 is slightly less inclined. It can also be seen from this figure that the cold-point, an estimate of the tropopause or transition from the active troposphere to the stable stratosphere, is significantly higher in SST302. The troposphere is 12 km deep in SST298 and 15 km deep in SST302. This will have inherent implications for the stability of the atmosphere (see Chapter VII).

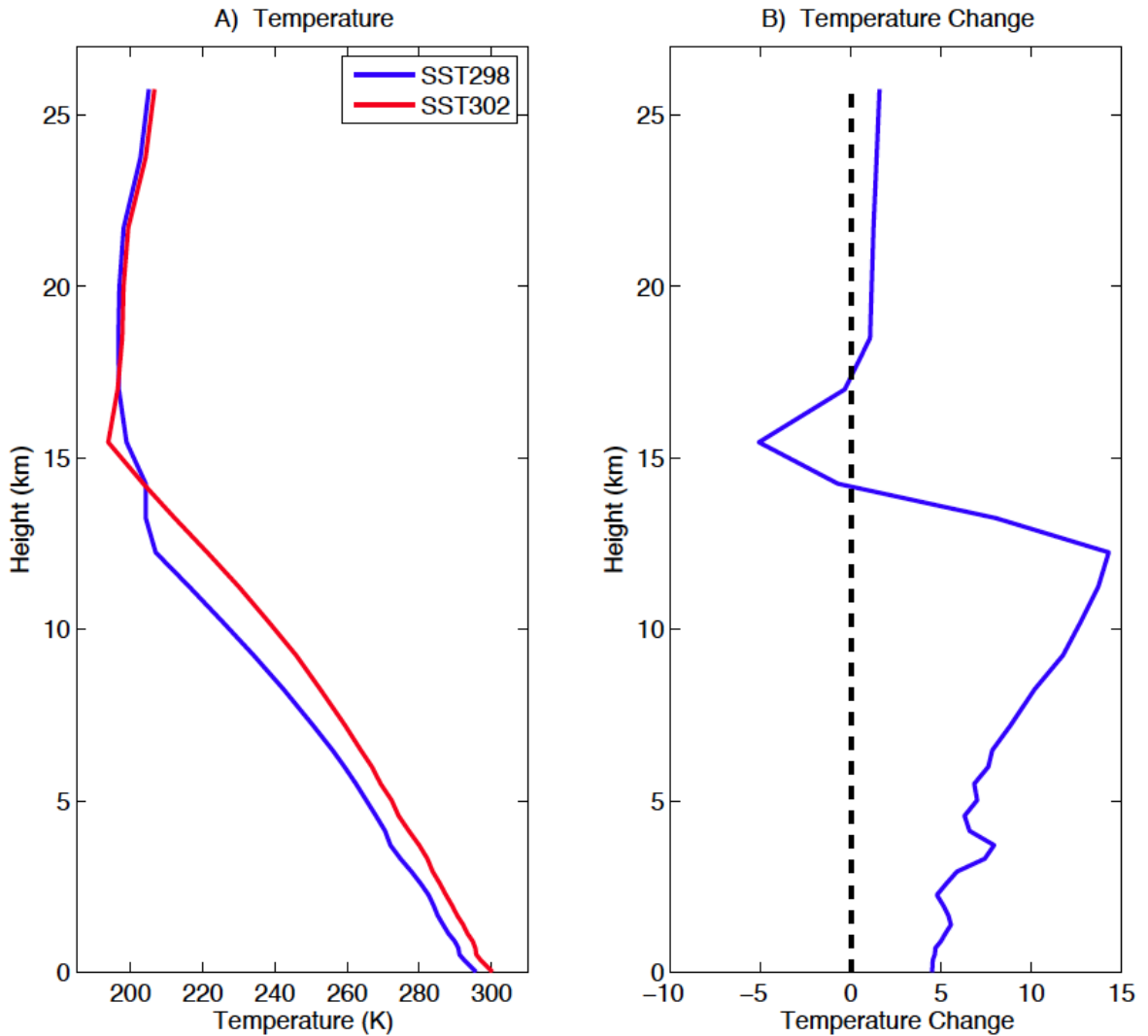


**Figure 2:** A) vertical profiles of domain and time averaged temperature from SST298 (blue) and SST302 (red). B) vertical profile of the averaged temperature differenced. Positive numbers indicate heights at which the simulation is warmer in SST302.

Unlike temperature, we do not know a priori how RH is likely to change with SST. It is generally found in GCMs and climate studies that RH remains approximately fixed as surface temperature changes (Ingram, 2002). There is some observational evidence for this assumption (Fitzjarrald and Garstang, 1981; Trenberth *et al.*, 2005). Figure 3, though, shows that in these simulations it does not remain constant. The format of Figure 3 is similar to Figure 2. It shows that while the shape of the RH profile

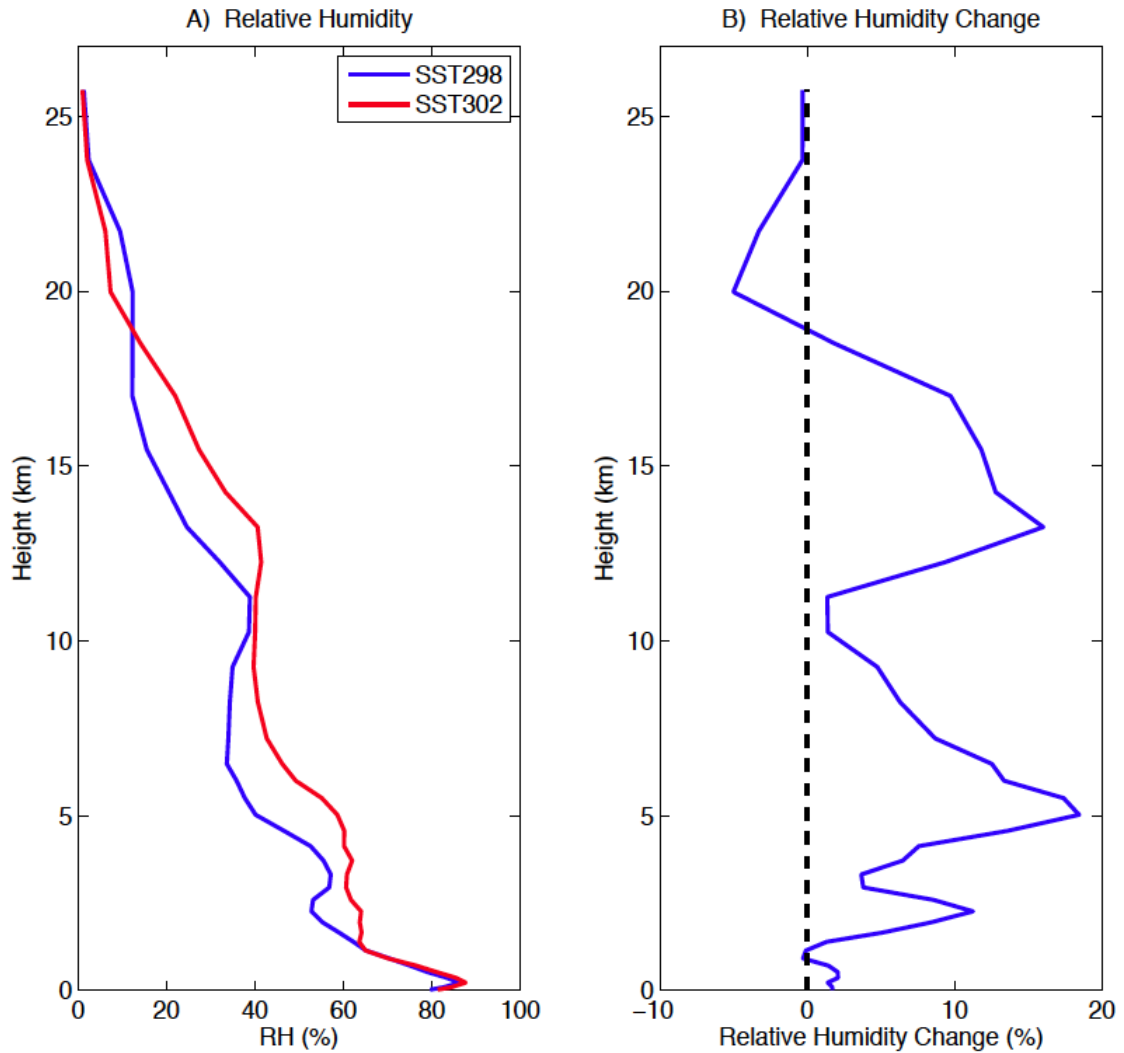


**Figure 3:** A) vertical profiles of relative humidity for SST298 (red) and SST302 (blue). B) vertical profile of the change in RH with SST.

retains most of its features while shifting vertically due to the deeper troposphere, the values of RH are higher in SST302 almost everywhere all the way up into the lower stratosphere (to 20km). The peak differences occur around the three detrainment levels of the trimodal distribution of clouds. There is both cause and effect in this occurrence as detrained clouds serve as a moisture source, but especially in the UT, the peak in RH influences the detrainment. The UT detrainment level maximum in total condensate correlates with the RH maximum there with coefficients of 0.93 and 0.90 in

SST298 and SST302, respectively. It should also be noted that an increase in RH with temperature inherently requires an increase in the total water vapor (increase in PW). The upper tropospheric RH change will be a crux of the arguments to come. It should also be noted that the increase in RH an increase in temperature implies an increase in PW. In fact the PW increases at just above the CC rate of

The upward cloud mass flux ( $M$ ) and the convective mass flux ( $M_c$ ) were computed at each model level following Robe and Emanuel (1996). At each level, the cloud mass flux is:

$$M = \rho \sum_{PW > PW_0, w > 0} \frac{N_c}{N} w_{i,j} = \overline{\rho w \sigma}. \quad (\text{EQ 4})$$

$N_c$  is the number of cloudy grid points at a level,  $N$  is the total number of grid points, and the summation is over points with an positive vertical velocity, and with the standard cloud mask applied for disturbed regions.  $\sigma$  is therefore a fraction of the domain with convection.  $M_c$  was calculated in the same way but over grid points with  $w > 1 \text{ m s}^{-1}$ . Figure 4 shows the  $M_c$  for SST298 and SST302. Both have an obvious peak in the lower troposphere, and SST298 has a strong peak around the level of upper level detrainment while in SST302 this peak is more subtle. The decrease in  $M_c$  with SST serves to imply that the average intensity of convection is reduced. This says nothing about individual convective cell intensity. The convective area fraction, is less in SST302 at nearly all levels up to the SST298 cold-point. Remarkably, the convective area fraction just below the tropopause, at the detrainment peak in both models, is much higher in SST298 than in SST302. At this

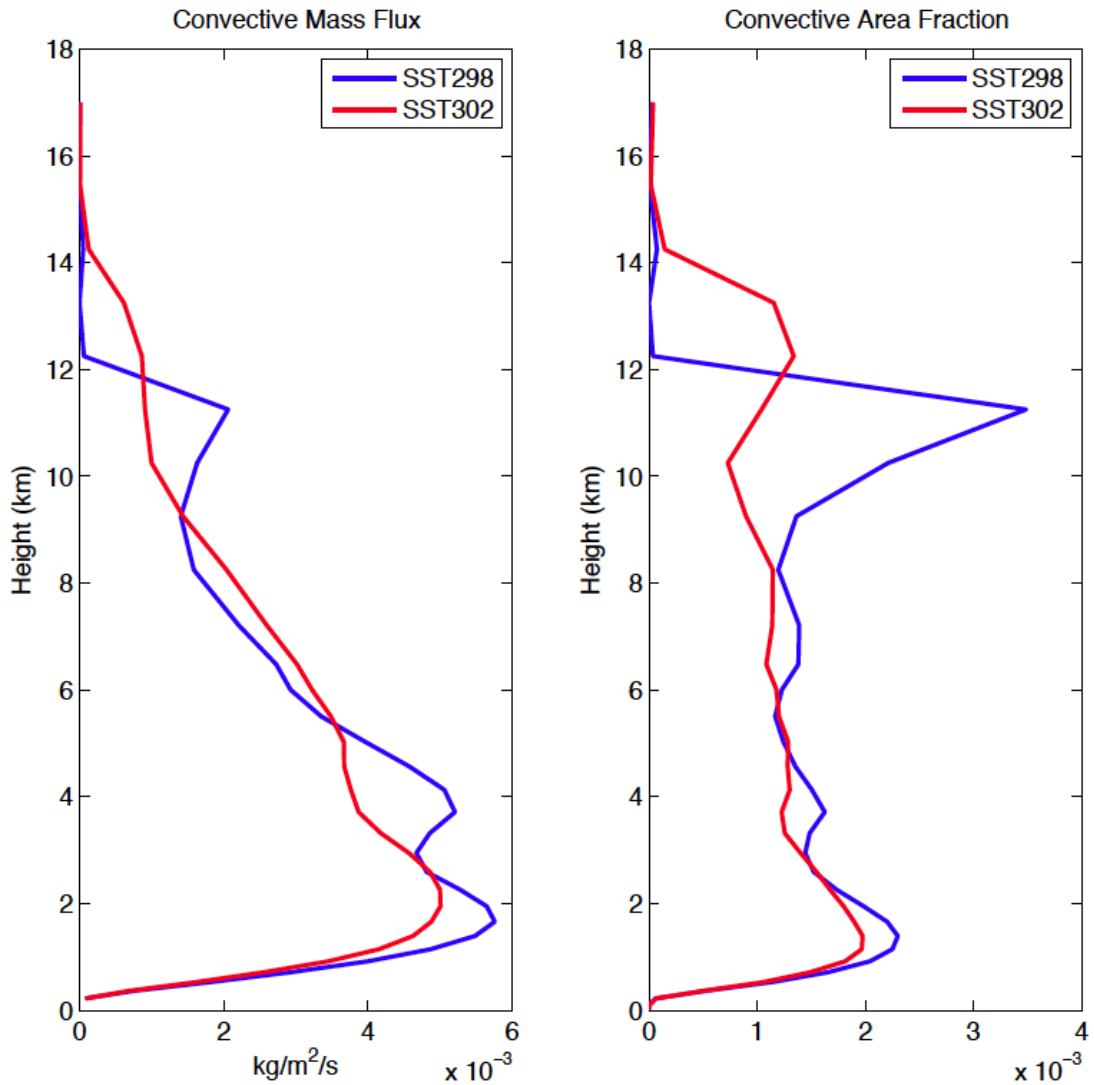


**Figure 4:** A) vertical profile of domain and time averaged convective mass flux. B) proportional area of convective area. In both, SST298 is in blue, and SST302 is in red.

point, the explanation for this is unclear, but it would seem to suggest more active UT convection in SST298.

### *Water Budget*

The analysis of the WV budget follows closely the technique used by van den Heever *et al.* (in press). Here it has been extended to the 3-dimensional model.

Analysis of water budget terms has been used previously to understand the effects of surface warming (Lau *et al*, 1993). The general WV conservation equation is:

$$\partial_t q + \vec{v} \cdot \vec{\nabla} q = e - c \quad (\text{EQ 5})$$

$q$  is the WV mixing ratio.  $e$  and  $c$  are the rates of evaporation and condensation per unit mass, respectively.  $\vec{v}$  is the 3-D wind vector. The flux form of the conservation equation can be obtained by utilizing the continuity equation and the product of Equation 5 with the air density,  $\rho$ . In 3 dimensions, it is:

$$\partial_t(\rho q) + \vec{\nabla} \cdot (\rho q \vec{v}) = \rho(e - c) \quad (\text{EQ 6})$$

Since we are interested in the behavior of WV binned by PW regimes, a column total quantity, Equation 6 needs to be integrated across the model's vertical domain:

$$\int_{z_b}^{z_t} \partial_t(\rho q) dz + \int_{z_b}^{z_t} \partial_x(\rho q u) dz + \int_{z_b}^{z_t} \partial_y(\rho q v) dz + \int_{z_b}^{z_t} \partial_z(\rho q w) dz = \int_{z_b}^{z_t} \rho(e - c) dz \quad (\text{EQ 7})$$

$z_b$  and  $z_t$  represent the model bottom and top layers, respectively.  $u$ ,  $v$ , and  $w$  are the standard Cartesian direction winds. Because the vertical wind must be zero at the model top and bottom, upon some rearranging of terms, Equation 7 becomes:

$$\partial_t \int_{z_b}^{z_t} \rho q dz = - \int_{z_b}^{z_t} u \partial_x(\rho q) dz - \int_{z_b}^{z_t} v \partial_y(\rho q) dz - \int_{z_b}^{z_t} \rho q \partial_x(u) dz - \int_{z_b}^{z_t} \rho q \partial_y(v) dz + E - P \quad (\text{EQ 8})$$

or

$$\partial_t \int_{z_b}^{z_t} \rho q dz = - \int_{z_b}^{z_t} \nabla_H(\rho q \vec{u}) dz + E - P \quad (\text{EQ 8'})$$

$\nabla_H$  is the horizontal gradient.  $\vec{u}$  is the horizontal wind vector. The left hand side of Equation 8 represents the local time rate of change of vertically integrated WV, or a

local rate of change of PW. The entire term will be analyzed as a PW storage term in what follows. The first two terms of the right hand side represent the advective contributions (ADV in Figure 5) and the second two terms represent the divergence contributions (DIV in Figure 5) of WV to the overall vertically integrated WV flux convergence. In the following, the effects of these two terms will be added as they are both grossly related to atmospheric motions. The final two terms are the surface evaporation, E, and surface precipitation, P. For a more complete description of the limitations of this type of analysis, see van den Heever *et al.* (in press).

While equation 8' does not contain any cross terms, and is therefore structurally similar to the 2-dimensional equation of van den Heever et al., the results of the analysis do expose some differences between the flux convergence characteristics of the 2-D and 3-D models.

Figure 5 illustrates the processes of Equation 8'. Taken piece by piece, the interaction of the WV flux and the disturbed/undisturbed dipole circulation can be seen. Advection and divergence is negative at low PW values characteristic of undisturbed regions and positive at high PW values characteristic of disturbed regions. This implies atmospheric motions serve to feed high PW regions with WV at the expense of WV from the low PW regions and sustains the moisture transport. Evaporation would seem to be the source of this moisture as it is positive in dry regions. Precipitation is the largest sink of WV out of wet regions. The storage term tells a more interesting story. For example, in SST298 the undisturbed region is defined to have PW of less than ~35mm. This can be easily inferred from Figure 5, but was defined to be

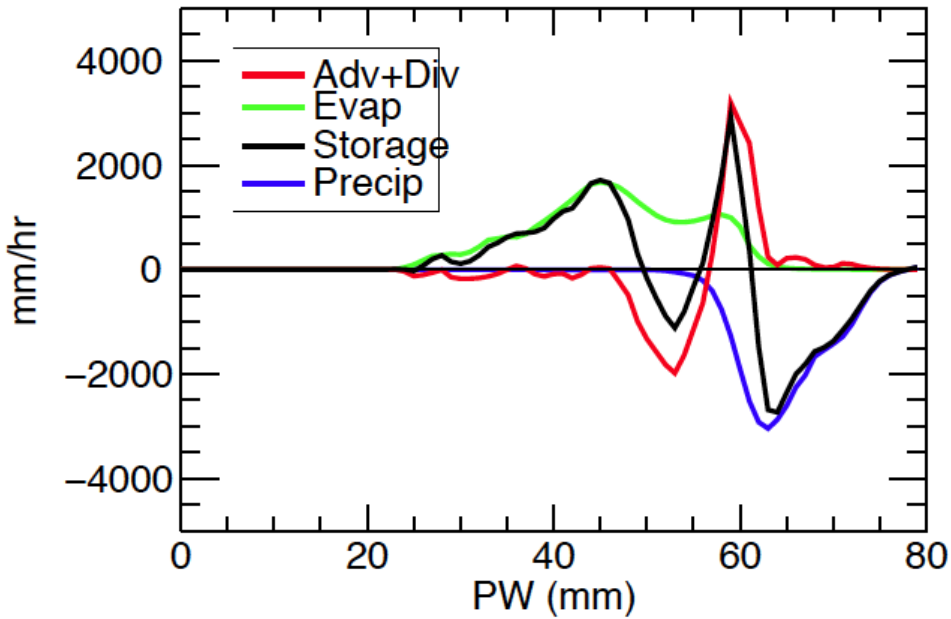
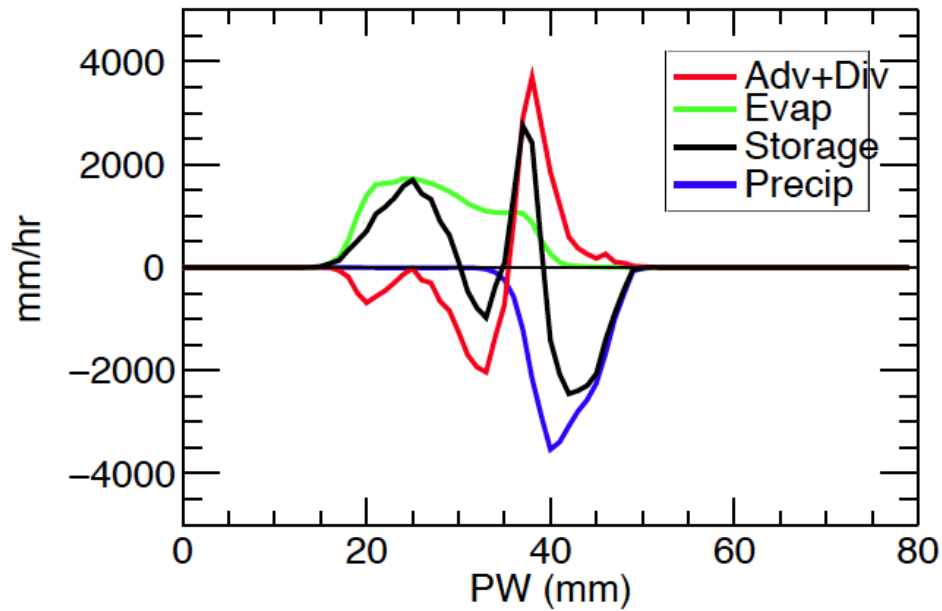


**Figure 5:** Total WV flux in  $\text{mm hr}^{-1}$  binned by PW. The upper panel is SST298 and the lower, SST302. The red line shows contributions from atmospheric motions. Positive (negative) values mean net gains (losses). The green line shows contributions due to evaporation (always positive). The blue line shows evacuation of WV through precipitation (always negative). The black line shows the sum of the previous three.

consistent with the OLR and condensate thresholds used elsewhere. The sign of the storage term below 35mm changes once. This sign flip implies that the driest parcels in the undisturbed regions gain WV from the surface and advect or diverge toward disturbed regions where they accelerate leaving a negative storage. Once in the disturbed regions, in this example at PW values above  $\sim 35$ mm, the WV accumulates due to convergence and advection before being rained out when PW gets too high. It should be noted that there is no forcing implies in Equation 8, only a balance. Terms can only interact in such a way as to maintain the balance, and in that sense do not cause one another. The vapor pathway described in this paragraph is only illustrative.

To first order, Figure 5 shows the rightward shift in PW space with SST mentioned in the last section. The second shift occurs within the components of the storage term respectively. Evaporation gains a local maximum within the disturbed region in SST302. The transition from the global minimum to maximum in divergence plus advection is slower in PW space in SST302. And, the precipitation sink falls off more slowly from its maximum in SST302. Taken together, these shifts imply a change in the interaction of these contributions. Local evaporation appears to influence wet regions more in SST302 than in SST298 while precipitation is not forced to fall as readily. This implies the reason for the moistening of the SST302 state – a lessened mean circulation (insofar as the evaporation shift may imply less surface wind) and much moister clouds (from precipitation shift).

### *Precipitation*

Though in many ways a silly argument, it is often stated that precipitation should increase at the same rate as PW (Wentz *et al*, 2007). If it doesn't, the WV cycling rate must decrease (Stephens and Ellis, 2008b). Because the mass flux arguments point to this fact, it may not be surprising that the modeled precipitation increases by only 2%  $K^{-1}$  when defined with respect to mean, column temperature – not the 7%  $K^{-1}$  of the CC relation similar to GCM climate models (Stephens and Hu, 2010). The total precipitation increase is a boundary condition since it is controlled by the surface flux scheme partitioning excess energy into sensible and latent heating. The way in which precipitation rates change is a more dynamically interesting story. Modeled rain rates exhibit a notable shift away from lighter rates ( $<1\text{mm hr}^{-1}$ ) toward higher ones ( $>5\text{mm hr}^{-1}$ ). Since the accumulated rain only changes by 4%  $K^{-1}$ , this shift toward higher rain rates requires a decrease in the total number of raining surface grid points.

The Figure 6 shows the rain rate binned by percentile of rain rate for both SST298 and SST302. On the right axis, the percent increase at each percentile is shown. While SST298 is above SST302 for most of the percentile spread which indicates the shift in SST302 away from light rain rates, SST302 is higher in the upper reaches of the percentile domain. This fact shows that at the heaviest rates, SST302 is yet more intensely raining than is SST298. This result has been examined in similar (e.g. Muller *et al*, 2011) studies as well as in dissimilar (e.g. Allen and Ingram, 2002) studies of modeled rain rate. The shift toward more intense rain events and away from the less intense has all kinds of implications for local rainfall climatology.

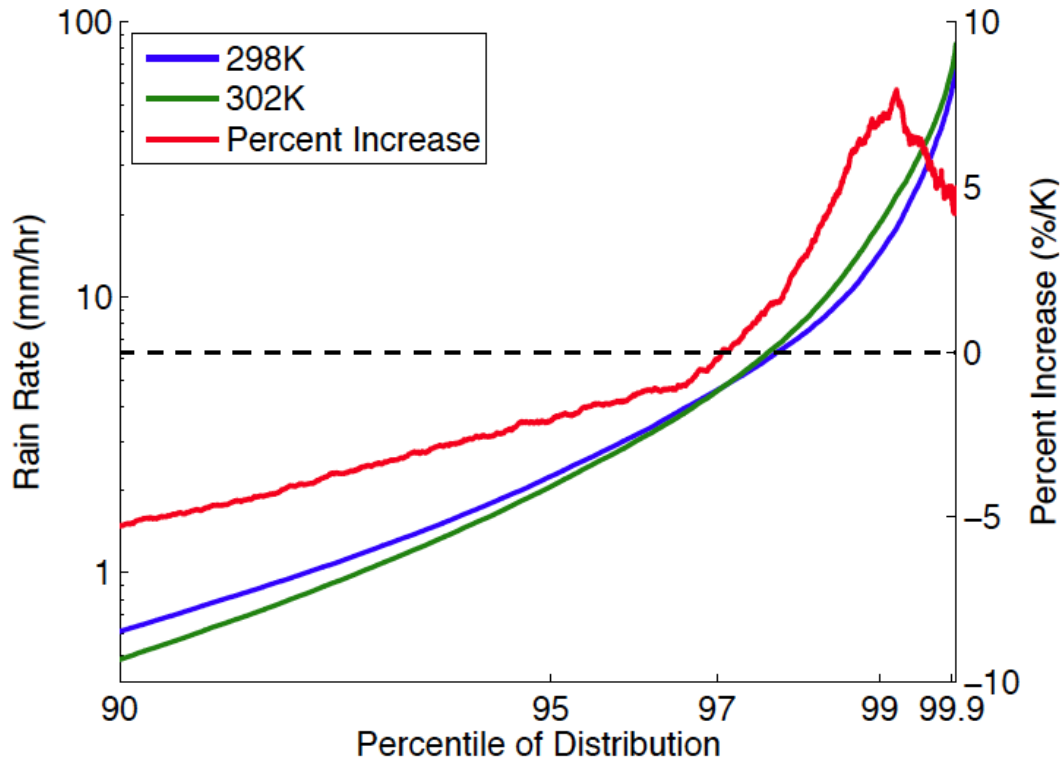


**Figure 6:** Rain rates for SST298 in blue and SST302 in green binned by percentile of rain rate on the left axis. In red on the right axis is the percent increase in rain rate for each rain rate percentile.

Figures 7 and 8 show PDFs of drizzle and rain binned by PW. Bins are 1 mm wide. Drizzle is defined as rain rates less than 1 mm hr<sup>-1</sup>; rain is greater than 1 mm hr<sup>-1</sup>. The magnitude of the PDF is the total percentage of the domain with drizzle or rain exhibited by a grid point with the shown PW. The characteristics of the PDFs show different behavior between the two SST states. SST298 seems to be more bimodal with a peak at low PW (undisturbed shallow convection) and at high PW (drizzle within disturbed regions). Rain peaks in a narrow range of PW values. SST302 seems to exhibit a slow ramp up in drizzle with PW before a quick increase in disturbed regions at the higher end of the PW range. Rain exhibits a slightly

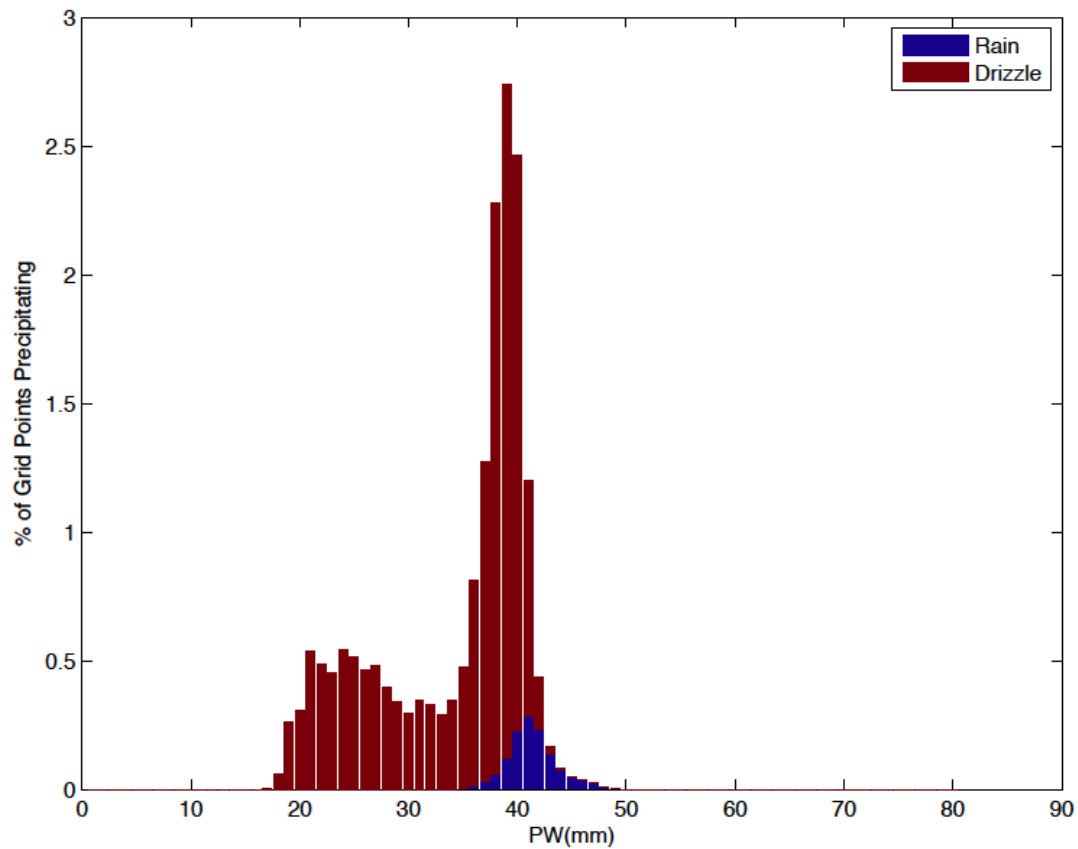


**Figure 7:** A probability density function of drizzle ( $<1 \text{ mm hr}^{-1}$ ) in maroon and rain ( $>1 \text{ mm hr}^{-1}$ ) in blue for SST298. The results are binned by precipitable water values.

wider peak in PW space than in SST298. It also has a notable tail to the right into very high PW regimes.

Figure 9 shows averaged rain rates binned by PW. There is an obvious separation in the PW values over which rain occurs in each experiment. This is due to the exponential dependence of the CC relation on temperature. The more interesting result is that SST302 seems to have access to much higher rain rates as a result of the regions of very high PW ( $>75 \text{ mm}$ ). Also, there is a PW region in SST302 at low values that exhibits a local maximum in rain rate. I do not have a

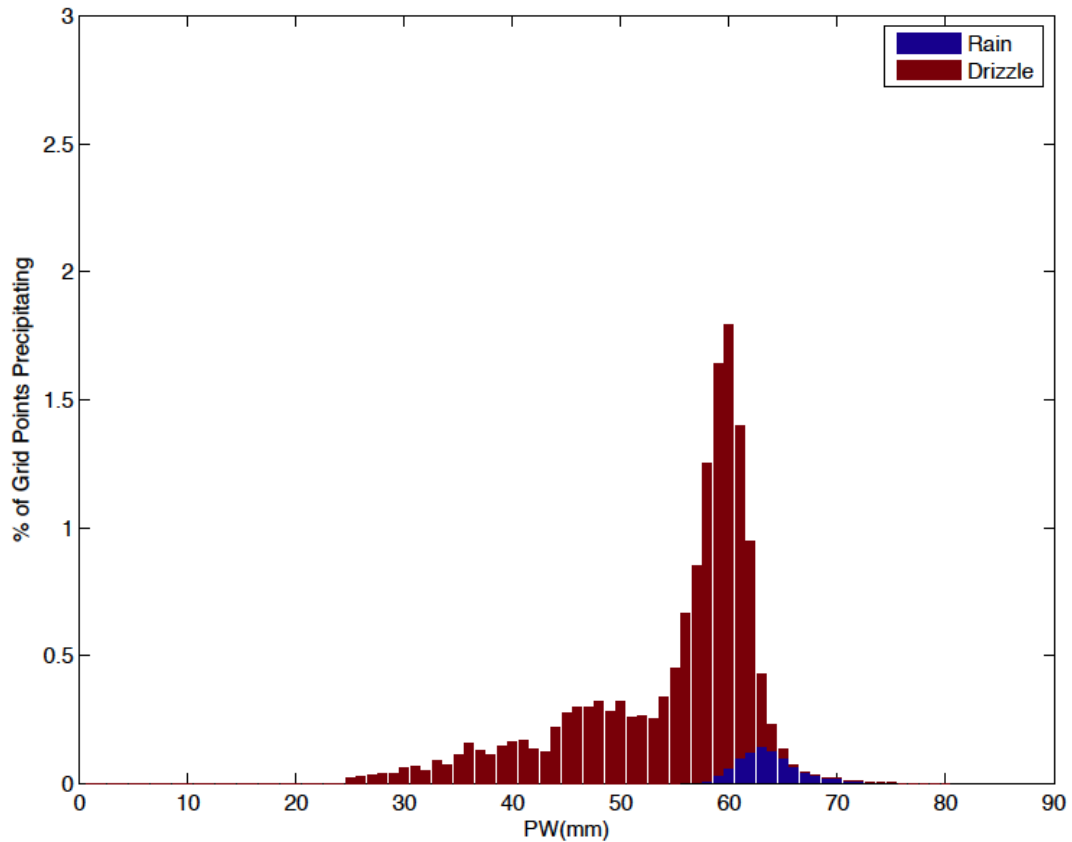


**Figure 8:** A probability density function of drizzle ( $<1 \text{ mm hr}^{-1}$ ) in maroon and rain ( $>1 \text{ mm hr}^{-1}$ ) in blue for SST302. The results are binned by precipitable water values.

clear explanation for why this exists other than that these PW values are probably characteristic of congestus regimes and that somehow the congestus precipitation is enhanced in SST302. Exploring this is beyond the scope of what has been analyzed in this study but could prove fruitful.

It is interesting to ask why precipitation changes the way it does. Of course it is a difficult question to answer definitively. Hopefully some light should be shed on this issue through the course of the analysis below.

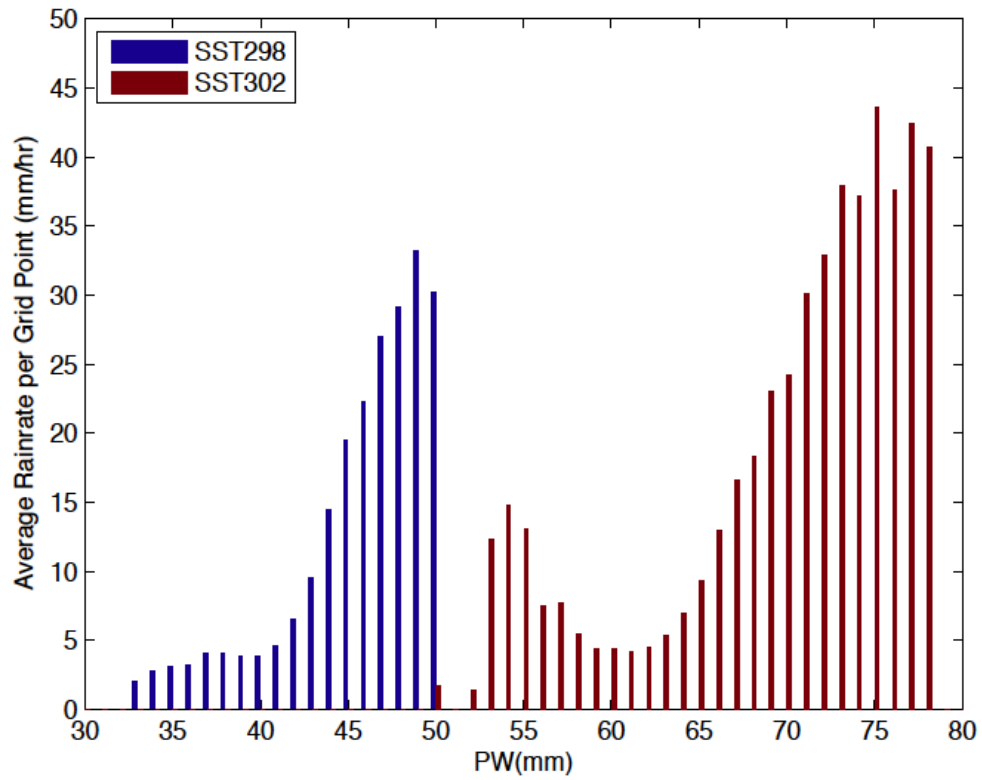


**Figure 9:** Average rain rate per grid point binned by PW. Blue bars show SST298 and maroon bars show SST302.

#### IV: THE POTENTIAL EFFECTS OF ENUMERATED CHANGES ON ANVILS

In the previous chapter, the reader was familiarized with how the overall model state changes with SST. This short chapter will seek to show how those changes form a coherent picture that will be relevant to TUT clouds and radiative feedbacks. While I have not yet even talked about how cloud properties change in the model, it is useful to develop an idea of how one might predict their changes.

The first hint at how TUT clouds might change comes from Figure 1. Since this is a plot of OLR, to a general extent, the figure shows the emission from cloud tops. The LW skin depth of clouds is small compared to the depth of UT modeled clouds, and as such cloud water is nearly opaque to many LW frequencies so emission from cloud top is a good assumption. Figure 1 shows that in addition to the physical size of the cloudy regions shrinking the variability within disturbed regions seems to increase. The standard deviation of OLR within disturbed regions increases from  $51.3 \text{ W m}^{-2}$  to  $52.0 \text{ W m}^{-2}$  and is statistically significant. This result would seem to imply some kind of change in either cloud structure or an increase in inter-cloud top height variability.

The convective mass flux, shown in Figure 4, and precipitation rate distribution may help to explain some of this. Total convective mass flux decreases with SST while the occurrence of heavy rain increases. These results would seem to be in direct contrast except that the  $M_c$  plots are a domain mean in excess of  $1 \text{ m/s}$  updrafts. So,

individual convective cells could gain strength with SST (stronger precipitation), but the total  $M_C$  can still go down. There is some evidence of this. The standard deviation of convective updraft intensity increases with SST from  $2.0 \text{ m s}^{-1}$  to  $2.5 \text{ m s}^{-1}$ . Since the distribution of convective velocities is a highly left skewed tail, this increase in standard deviation indicates an increased occurrence of infrequent, intense events. In such a case, the increased variability of convective strength between storms could, in principle, result in increased cloud top variability. Figure 2 shows that the temperature of the minimum point in the temperature profile decreases with increased SST. This would allow lower temperatures to be easily accessible to cloud tops still within the tropopause.

The water budget and RH plots help to shed light on the availability of WV to detrain and to form anvils. Figure 3 clearly shows an increase in RH in the UT in SST302. The WV budget calculations help to explain why it might be there. The storage at PW values typical of anvil regions is slightly higher in SST302. Due to the logarithmic nature of water vapor concentrations with height, Figure 5 mostly shows lower tropospheric processes. Therefore, the storage term can help to shed some light on sink regions at heights with low concentrations of WV. Though not shown here, a companion plot to the WV budget figure showing calculations done only in the UT confirms that there is greater flux out of high PW regions in SST302 than in SST298.

To summarize, the convective circulation, in an average sense, decreases with SST while individual convective cell intensity increases as inferred from the increase in intensity of high rain rates. This might lead to the increased variability of UT clouds. WV is more effectively cycled out of the tops of disturbed regions due presumably to the

decrease in average convective intensity which leads to a more moist UT. The episodic intense convection is taken to be a strong moisture source that the lessened mean circulation is less likely to advect toward the surface.

## V: THE TUT RADIATION DEPENDENCE ON RH

The RH increase with SST in the UT is the result of dynamics, but it has a profound effect on the radiative profiles of the modeled atmosphere because WV effectively controls tropospheric LW. A formulation will be derived that seeks to illuminate the UT dependence on WV in general and on RH more specifically. It was shown in chapter II that a local cooling in the TUT leads to subsidence and cloud detrainment. The basic formulations below are derived from Soden and Bretherton (1993) and Stephens *et al* (1996).

Transmission of WV can be assumed to follow a square-root dependence on WV path. That is:

$$T_R = k[u(p)]^{1/2} \quad (\text{EQ 9})$$

where  $T_R$  is transmission,  $k$  is some contextually dependent constant,  $u$  is the WV concentration, and  $p$  is pressure. The WV path is:

$$u(p) = \frac{18}{29} \int_0^p RH(p') \frac{e_s dp'}{p' g} = \frac{18}{29} \int_0^p RH(p') \frac{e_s}{g} d \ln p' \quad (\text{EQ 10})$$

where  $g$  is gravity and  $e_s$  is the saturation vapor pressure. In changing the integral to one over height,  $z$ ,  $u(p)$  becomes:

$$u(p) = u(z) = \frac{-18}{29} \int_{\infty}^z RH(z') \frac{e_s}{g H} dz' \quad (\text{EQ 11}).$$

The constant H is the atmospheric scale height and g is the Earth's gravitational constant.  $e_s$  can be defined as:

$$e_s(T(z)) = e_s(T_0) * e^{(\lambda(T(z)-T_0)/T_0)} \text{ (EQ 12).}$$

$T_0$  is a reference temperature of 300K,  $T(z)$  is temperature, and  $\lambda$  is 12.6. These are non-standard constants. They were found by fitting Equation 16 to the modeled heating rates in SST298 and SST302 with a simple least squares fit. See Chapter VI for a simple assessment of the success. Placing this into the equation for  $u(z)$  shows:

$$u(z) = \frac{18}{29} \frac{e_s(T_0)}{gH} \int_z^\infty RH(z') * e^{(\lambda(T(z')-T_0)/T_0)} dz' \text{ (EQ 13).}$$

One may get a formula for transmission by substituting this form of  $u(z)$  into the square root dependence above, Equation 9. This shows explicitly that  $T_R$  is a function of RH. Transmission to space is the dominant contribution to local heating, or in this case cooling, in the TUT (Harries, 1996). The heating rate as a function of height may be calculated from  $T_R$  as:

$$H(z) = \frac{-1}{\rho C_p} \pi B(z) \frac{dT_R}{dz} \text{ (EQ 14)}$$

where  $C_p$  is the isobaric specific heat and B is the thermal emission. The vertical gradient of  $T_R$  is:

$$\frac{dT_R}{dz} = k \frac{1}{2} [u(z)]^{-1/2} \frac{d}{dz} [u(z)] = k \frac{1}{2} [u(z)]^{-1/2} * \left[ \frac{18}{29} \frac{e_s(T_0)}{gH} RH(z) * e^{(\lambda(T(z)-T_0)/T_0)} \right] \text{ (EQ 15).}$$

Substituting in all known quantities gives:

$$H(z) = \frac{-1}{\rho C_p} \pi B(z) k \frac{1}{2} \left[ \int_z^\infty RH(z') * e^{(\lambda(T(z')-T_0)/T_0)} dz' \right]^{-1/2} * \left[ \left( \frac{18}{29} \frac{e_s(T_0)}{gH} \right)^{1/2} RH(z) * e^{(\lambda(T(z)-T_0)/T_0)} \right] \text{ (EQ 16).}$$

Thus the heating (cooling) of the TUT is directly dependent on the local RH. Equation 16 also exhibits a variety of other dependencies including several implicit and explicit dependencies on temperature. It was never the intention to disprove the notion that the local heating rate is dependent on temperature; only that it was not solely dependent on temperature.

In the formulation of the FAT hypothesis, this dependence on RH is implicitly assumed to be insignificant. That is worth testing however since Equation 16 has been derived. To test the sensitivity of RH of Equation 16, a simple toy mathematical model with a constant lapse rate of  $\Gamma_{RCE}$ , a 15km tropopause, a WV content dictated by the CC relation and two constant values of RH was developed. One WV vapor profile used a constant RH of 40%, the other, 50%. These values are quite low for much of the tropical troposphere but representative of UT RH in SST298 and SST302 and in nature (Ryoo *et al*, 2009). The increase from 40% to 50% in RH resulted in a peak, UT cooling increase of 9%. This result shows that Equation 16 is potentially quite sensitive to total RH.

Since Equation 14 depends on the vertical gradient of T, the sharp peak in atmospheric cooling is the result of the concentration of WV going to zero very quickly with height. As such, another use of this simple model was to arbitrarily set the WV concentration to zero below some threshold of WV at which it may be assumed that cooling by WV is negligible. Because RH dictates where this transition occurs, the peak cooling is forced to different levels in the different RH cases. The 10% increase in RH moved the level of peak cooling down in temperature space by 2.2 K. The blackbody emission decrease from this transition would be about  $5 \text{ W m}^{-2}$ .

Insofar as a single column model that interacts with radiation only through a WV concentration is representative of the physics in Equation 16, these are results that would seem to indicate a high sensitivity to RH, not just to temperature. It is undeniable that changing the temperature profile in this model has a profound effect on the results, but it is not the only constraint. A control of UT heating by some factor other than temperature means that for a given temperature the local heating rate can vary depending on local and, more weakly, on above column RH. If UT heating is not constrained solely by temperature, then neither is the detrainment peak.

In the Sensitivity section (next), the rate of change of UT heating with respect to unit changes in temperature and RH has been derived. The results show that changing the local temperature by 1 K has the same effect on heating as changing the local RH by 10% (i.e. a change from, for example, 40% to 50%, not from 40% to 44%). As a rough estimate from Figure 2, the change in UT temperature between SST302 and SST298 is on the order of 10 K. Figure 3 shows that the change in UT RH is on the order of 10%. Those numbers imply that the change in UT radiative cooling with SST is driven by 1 part in 10 by the change in UT RH. This explains why FAT is approximately true. Most of the variability in the DC peak in the UT is controlled by temperature. But, if the CSRМ study is truly representative of the climate state of the tropics with respective SSTs, then one could expect slightly cooler anvil temperatures (CAT) with increasing SSTs.

The results of Equation 16 have been tested against the full radiation code of BugsRad. The BugsRad model is a two-stream model that calculates molecular scattering and gaseous absorption (Stephens *et al*, 2001) the latter of which is done through the correlated k distribution of Fu and Liou (1992). A standard BugsRad clear

sky, tropical profile was used. A comparison was made between two profiles each with constant relative humidity of either 40% or 50% within the troposphere. The peak UT cooling increased by 17% when the relative humidity was raised from 40 to 50 percent. This is a slightly higher sensitivity than the results from Equation 16. A profile that was 1 K warmer at every level was run through BugsRad in an attempt to assess the results presented in the previous paragraph. The warmer state only cooled by 2% more. The results derived in the Sensitivity section suggest that a 1 K increase in temperature should have had approximately the same effect as increasing the RH by 10%. This is obviously not the case in BugsRad where the sensitivity is even higher to RH. The discrepancy could come from any one of a number of assumptions that go into calculating the approximation in the Sensitivity section. However, these results only serve to emphasize the potential importance to UT cooling of changing RH.

### *Sensitivity*

In this section the rate of change of upper tropospheric heating rate with respect to both relative humidity and temperature will be assessed. As a reminder, the heating rate, Equation 16 is:

$$H(z) = \frac{-1}{\rho C_p} \pi B(z) k \frac{1}{2} \left[ \int_z^{\infty} RH(z') * e^{(\lambda(T(z')-T_0)/T_0)} dz' \right]^{-1/2} * \left[ \left( \frac{18}{29} \frac{e_s(T_0)}{gH} \right)^{1/2} RH(z) * e^{(\lambda(T(z)-T_0)/T_0)} \right]$$

(EQ 16).

Next, the rate of change of heating with respect to RH is:

$$\frac{\partial H(z)}{\partial RH(z)} = \frac{-1}{\rho C_P} \pi B(z) \left( \frac{18 e_s(T_0)}{29 gH} \right)^{\frac{1}{2}} e^{\lambda(T(z)-T_0)/T_0} * \frac{\partial}{\partial RH(z)} (RH \left[ \int_z^\infty RH(z') e^{\lambda(T(z)-T_0)/T_0} dz' \right]^{-\frac{1}{2}})$$

(EQ 17).

Some short hand will be employed.  $\gamma_{RH}$  will equal the pieces of Equation 17 preceding the partial derivative that do not depend on RH.  $\alpha$  will equal the pieces that are in the exponential.  $\beta$  will equal the integral. As such Equation A1 can be rewritten as:

$$\frac{\partial H(z)}{\partial RH(z)} = \gamma_{RH} * \frac{\partial}{\partial RH(z)} (RH \left[ \int_z^\infty RH(z') e^\alpha dz' \right]^{-\frac{1}{2}}) = \gamma_{RH} * \frac{\partial}{\partial RH(z)} (RH[\beta]^{-\frac{1}{2}}) \quad (\text{EQ 18})$$

On taking the derivative, Equation 18 becomes:

$$\frac{\partial H(z)}{\partial RH(z)} = \gamma_{RH} * (1 * \beta^{-\frac{1}{2}} + RH(z) * \frac{1}{\partial RH(z)/\partial z} * \frac{\partial}{\partial z} [\beta^{-\frac{1}{2}}]) \quad (\text{EQ 19}).$$

The partial derivative of  $\beta$  is:

$$\frac{\partial \beta}{\partial z} = [-RH(z) \frac{\lambda}{T_0} e^\alpha \frac{\partial T(z)}{\partial z} - e^\alpha \frac{\partial RH(z)}{\partial z}] \quad (\text{EQ 20}).$$

Thus, Equation 19 becomes:

$$\frac{\partial H(z)}{\partial RH(z)} = \gamma_{RH} * (\beta^{-\frac{1}{2}} + RH(z) * \frac{-\frac{1}{2}}{\partial RH(z)/\partial z} * [-RH(z) \frac{\lambda}{T_0} e^\alpha \frac{\partial T(z)}{\partial z} - e^\alpha \frac{\partial RH(z)}{\partial z}]^{-\frac{3}{2}})$$

(EQ 21)

Next, the partial derivative with respect to temperature will be assessed. The same shorthand will be used and redundant steps left unwritten. It is:

$$\frac{\partial H(z)}{\partial T(z)} = \frac{-1}{\rho C_P} \pi \left( \frac{18 e_s(T_0)}{29 gH} \right)^{\frac{1}{2}} RH(z) * \frac{\partial}{\partial T(z)} (B(T(z)) * e^\alpha * [\beta]^{-1/2}) \quad (\text{EQ 22}).$$

$\gamma_T$  will be taken to mean those pieces of Equation 22 before the partial derivative. If  $B(T(z))$  is assumed to be the Stefan-Boltzmann emission,  $\sigma T^4$ , then upon taking the derivative, Equation 22 becomes:

$$\frac{\partial H(z)}{\partial T(z)} = \gamma_T (4\sigma T^3 e^\alpha [\beta]^{-\frac{1}{2}} + B(T(z)) \frac{\lambda}{T_0} e^\alpha [\beta]^{-\frac{1}{2}} + B(T(z)) e^\alpha \frac{-\frac{1}{2}}{\partial T(z)} \left[ -RH \frac{\lambda}{T_0} e^\alpha \frac{\partial T}{\partial z} - e^\alpha \frac{\partial RH}{\partial z} \right]^{-\frac{3}{2}}) \quad (\text{EQ 23}).$$

Now that both of these dependencies have been derived. I seek to assess their relative importance. This will be accomplished by taking their ratio:

$$\frac{\frac{\partial H(z)}{\partial RH(z)}}{\frac{\partial H(z)}{\partial T(z)}} = \frac{\gamma_{RH} * (\beta^{-\frac{1}{2}} + RH(z)) * \frac{-\frac{1}{2}}{\partial RH(z)/\partial z} * \left[ -RH(z) \frac{\lambda}{T_0} e^\alpha \frac{\partial T(z)}{\partial z} - e^\alpha \frac{\partial RH(z)}{\partial z} \right]^{-\frac{3}{2}}}{\gamma_T (4\sigma T^3 e^\alpha [\beta]^{-\frac{1}{2}} + B(T(z)) \frac{\lambda}{T_0} e^\alpha [\beta]^{-\frac{1}{2}} + B(T(z)) e^\alpha \frac{-\frac{1}{2}}{\partial T(z)} \left[ -RH \frac{\lambda}{T_0} e^\alpha \frac{\partial T}{\partial z} - e^\alpha \frac{\partial RH}{\partial z} \right]^{-\frac{3}{2}})} \quad (\text{EQ 24}).$$

Equation 24 can be simplified by recognizing that  $\gamma_{RH}$  equals  $\gamma_T * B(T(z))$ .

Additionally,  $\delta$  will be taken to be the pieces raised to the  $-3/2$ . Finally the ratio of the derivatives is:

$$\frac{\frac{\partial H(z)}{\partial RH(z)}}{\frac{\partial H(z)}{\partial T(z)}} = \frac{\beta^{-\frac{1}{2}} + RH(z) * \frac{-1/2}{\partial RH(z)/\partial z} * [\delta]^{-3/2}}{e^\alpha ([\beta]^{-\frac{1}{2}} (\frac{4}{T(z)} + \frac{\lambda}{T_0}) + \frac{-1/2}{\partial T(z)/\partial z} [\delta]^{-\frac{3}{2}})} \quad (\text{EQ 25}).$$

Equation 25 actually depends on very few things for being so complex. It depends on local RH and temperature, their vertical gradients, and their above column integrals. Some scale analysis with broadly representative numbers taken

from the model output can be used to assess Equation 25. The right hand side of Equation 25 computes to approximately 10. For a unit change in heating rate, the derivatives may be thought of as discrete changes such that:

$$\frac{\Delta H / \Delta RH}{\Delta H / \Delta T} \approx 10 \text{ (EQ 26),}$$

or:

$$\Delta T \approx 10 \Delta RH \text{ (EQ 27).}$$

As such, a 10% (0.10) change in RH effects approximately the same change in heating as does a 1 K change in temperature.

## VI: SIMULATED UT RADIATIVE PROCESSES

Chapter V showed that in a simple framework, RH can affect UT cooling rates. But what about in a more complex mathematical simulation such as SST298 and SST302? It has already been shown that some characteristics, especially temperature and RH, do change with SST in the simulated UT. And since these variables affect radiation, it would seem probable that UT radiation could change.

Figure 10 shows the clear sky LW cooling profile in SST298 and SST302 in solid lines. The dashed lines are the results from Equation 16 using state variables from the SST experiments as inputs averaged by SST. The results using Equation 16 can be seen to be rather representative in the UT especially of the vertical gradient of heating rate. The mean square difference between the modeled results and the results from Equation 16 are only 0.8. Examining the modeled results again, the normal vertical shift in the height of features with SSTs is readily apparent. It is also notable that the shape of the profile changes, and that neither is especially well representative of the theoretical profile (Salby, 1996) in the lower troposphere, due to water vapor continuum effects, though they are close enough to maintain the detrainment controls which are central to this work (shown next). The UT cooling maximum increases from  $2.0 \text{ K day}^{-1}$  to  $2.3 \text{ K day}^{-1}$ . This increase acts to destabilize the clear sky regions. Except for some subtle differences, the profiles from SST298 and SST302 are similar in the lower troposphere

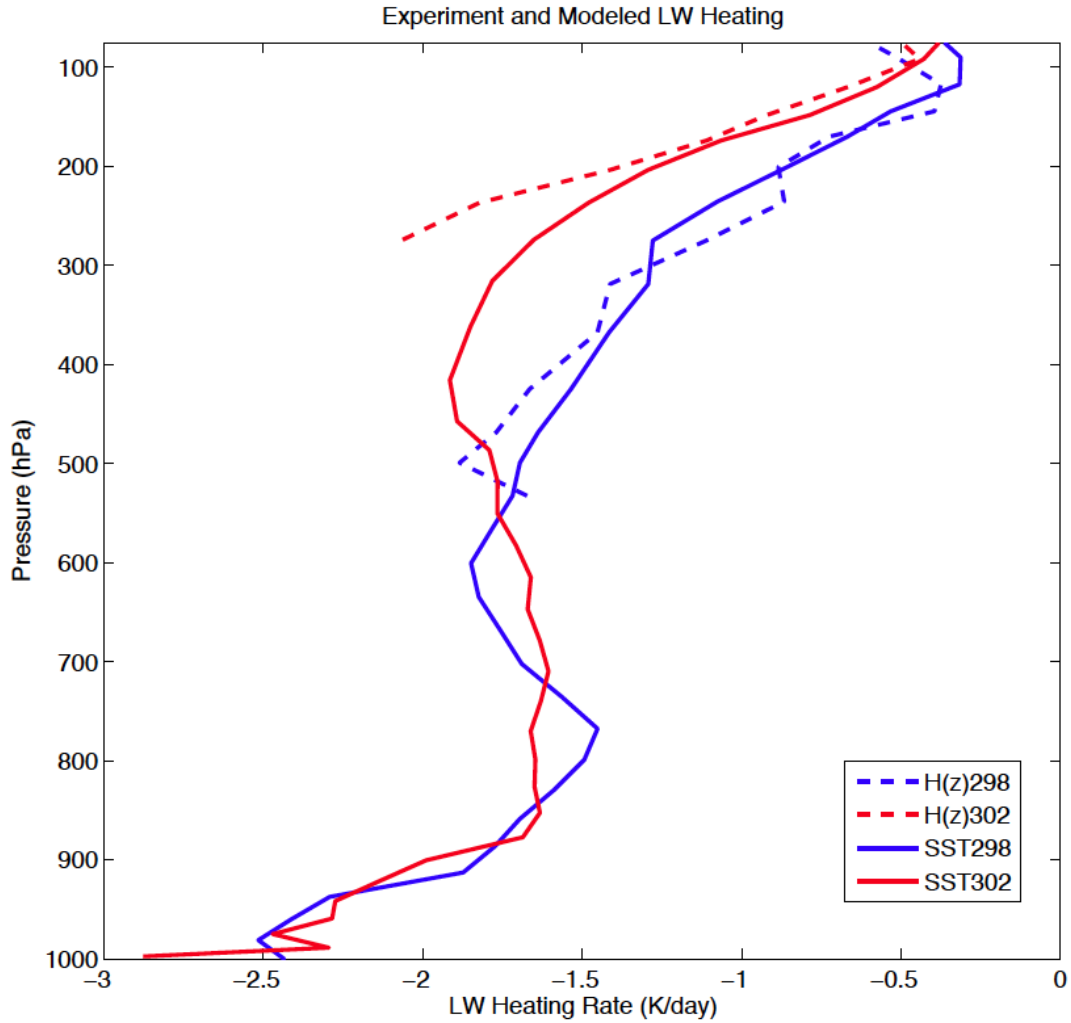


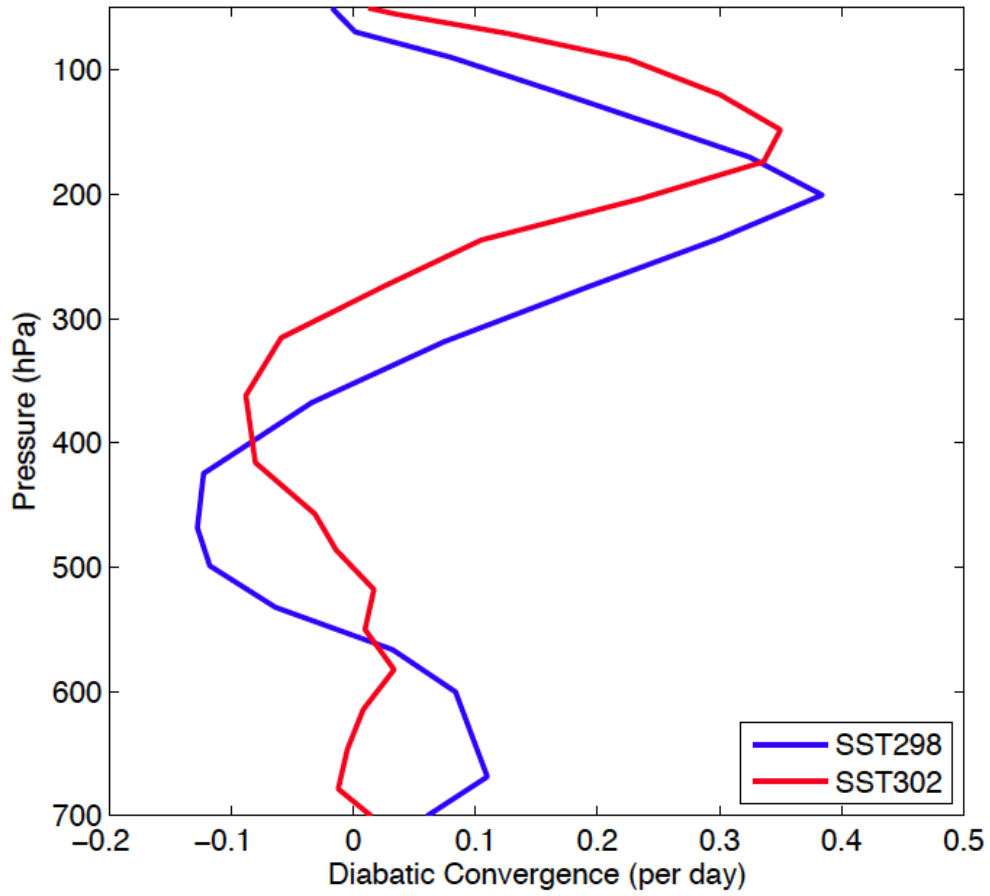
**Figure 10:** The modeled LW heating rates versus pressure in undisturbed, clear sky regions only. SST298 is in blue; SST302 is in red. The dashed lines show the results from Equation 16 using environmental variables from SST298 and SST302 to populate the parameter space.

which suggests that radiation plays an insignificant role in any dynamic changes there. The total cooling is greater in SST302. This makes sense given the inherent controls of total cooling on total precipitation (Allen and Ingram, 2002) which was shown to increase by  $2\% \text{ K}^{-1}$ .

Having examined the LW cooling, it is possible to derive the modeled diabatic convergence (DC) through Equations 1-3. Cooling to space is by far the largest

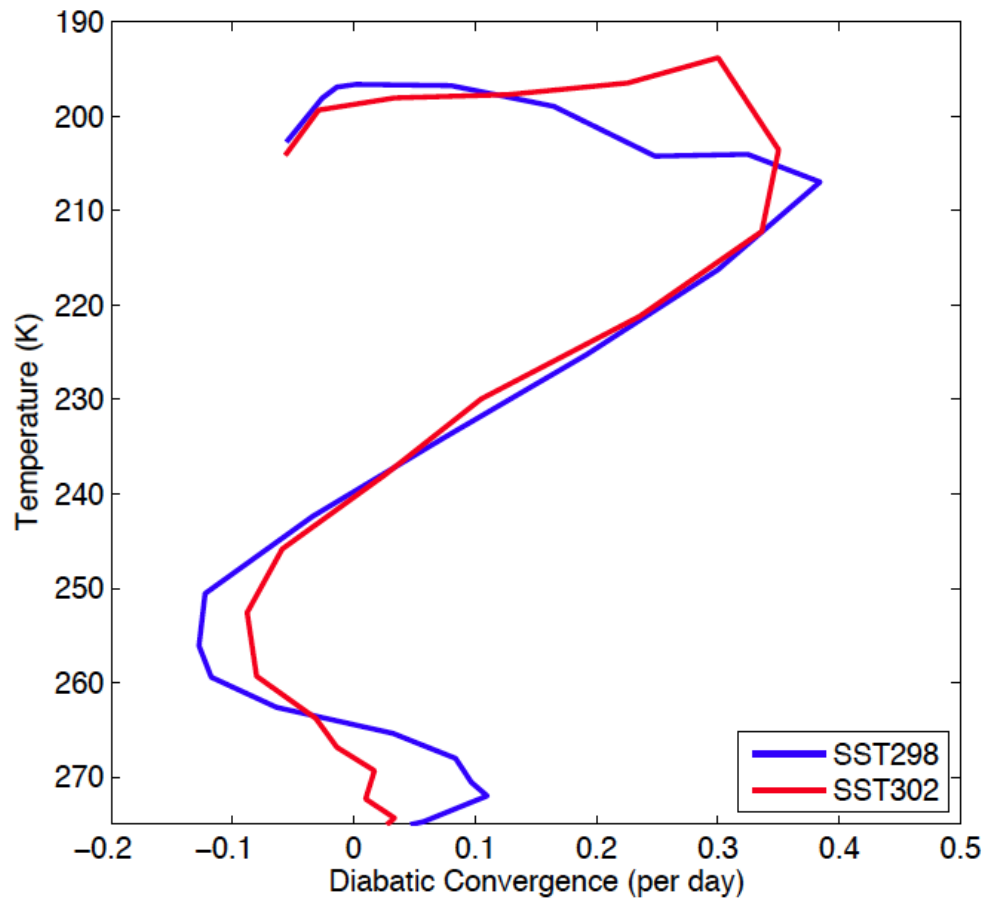
contribution to TUT cooling, and so, these calculation are at least first order accurate. Figure 11 shows the DC profiles of SST298 and SST302 calculated from the modeled state for pressures lower than 700 hPa. The figure only includes these pressure levels because the derivation is only valid in the UT where WV continuum effects are insignificant. The sharp peak in DC is expected (as above), and its calculated existence lends some credence to the results even though the cooling profiles do not exactly fit theory as the maximum in SST298 is down around 700hPa. As usual, features shift downward in pressure space (i.e. to lower pressure) with increasing SST. Additionally, though, the shape of the DC peak in the UT changes. The DC peak is both lesser and smoother in SST302. Like the decreased convective fluxes, the DC implied circulation would seem to hint at a less robust movement of mass with increasing SST. The DC distribution in SST302 broadens with respect to its peak. The standard deviation of the DC distribution modestly increases from 0.17 to 0.21. This could point to a broader but less intense detrainment maximum in the UT.

Figure 12 shows the same DC as Figure 11 except now in temperature space. Most of the profile can be seen to be strongly controlled by temperature as the profiles lie on top of one another. Colder than  $\sim 215$  K, however, the profiles are quite different. Suggesting more temperature dependent detrainment, the DC peak is much sharper in SST298 than in SST302. It is also slightly higher in SST298. It would seem that detrainment would be confined in SST298 to a narrow range of temperatures centered on the peak in DC of 207K. While in SST302, the detrainment could occur in a wider range of temperatures centered on the DC peak at 203K. The change in temperature



**Figure 11:** Profile of the domain and time averaged diabatic convergence. SST298 is in blue; SST302 is in red.

space of the DC maximum with SST is in direct conflict with the Fixed Anvil Temperature Hypothesis and is reflective of the results in Chapter V.



**Figure 12:** Profile of domain and time averaged diabatic convergence. Results from SST298 and SST302 are in blue and red, respectively.

## VII: MODEL SUBSIDENCE REGIONS

The decrease in DC strength and the lessened convective fluxes show that the domain mean circulation within the disturbed regions decreases with SST. These arguments would seem to imply a change in the undisturbed region circulation. If a change in the undisturbed region is such that it, in turn, implies the changes in the disturbed region circulations, a nice feedback loop could be established. This will be the endeavor undertaken in this chapter.

It was mentioned in chapter II that although the modeled subsidence regions are marked by levels of increased stability that relate in some way to the RH maximums created by cloud detrainment or the boundary layer. Circulations set up due to these stable regions such that air subsides into them increasing their stability. The circulations help control the RH gradient and the stable regions are self-sustaining.

Figure 13 shows an example model subsidence region from SST298; Figure 14 shows SST302. The filled contours are the meridionally averaged vertical gradient of potential temperature. Regions over  $4 \text{ K km}^{-1}$  are taken to be statically stable insofar as they are not potentially unstable. The open white contours are the maximum value of total condensate along the meridional direction. The horizontal axis labels grid points in the zonal direction. Pixels 1000 to 1500 were chosen because they coincided with the edges of disturbed regions in both SST298 and SST302 at the final time step.

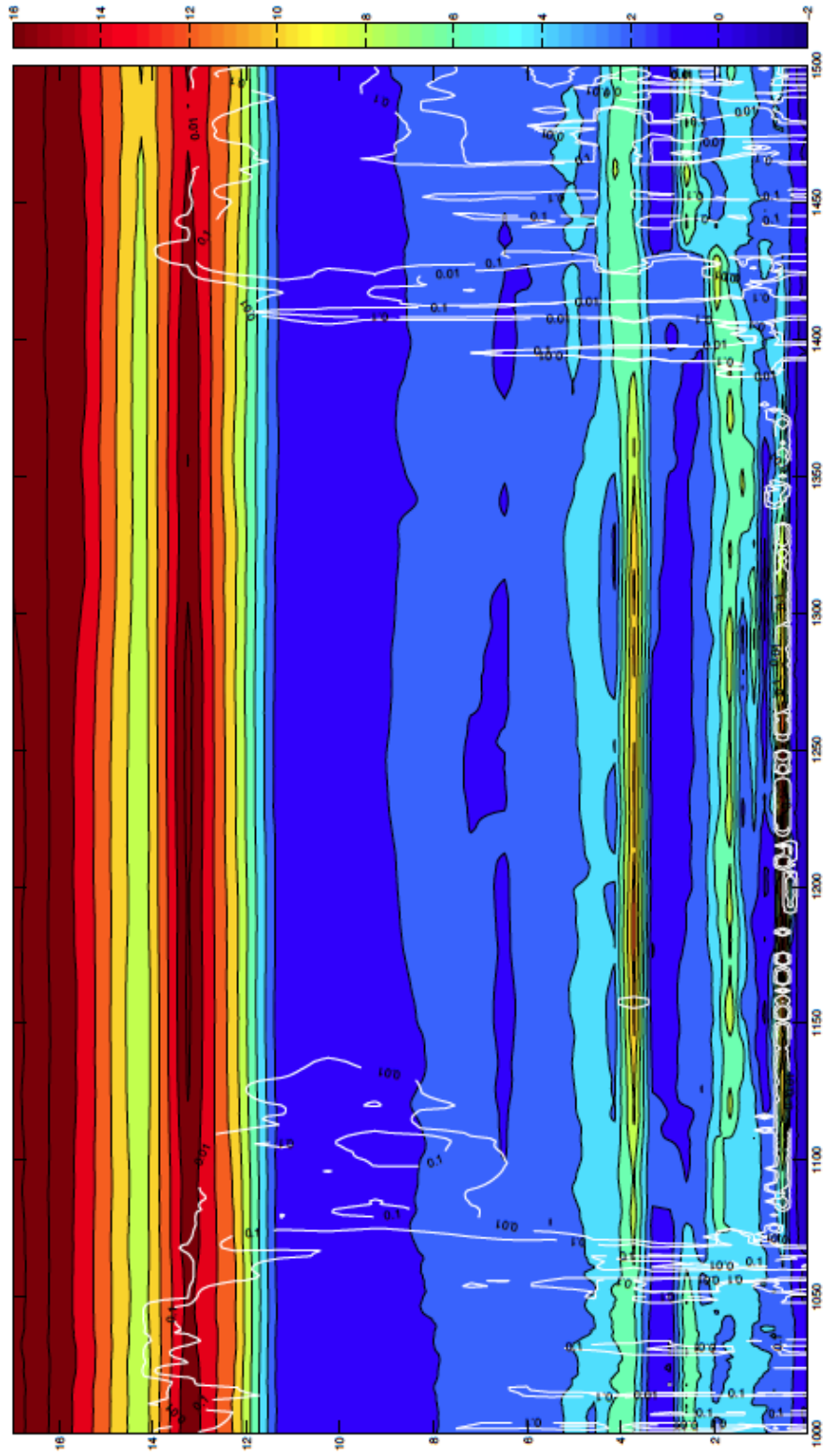


**Figure 13:** Filled contours are potential temperature lapse rate. Open contours are maximum value of total condensate mixing ratio along the meridional direction – they outline clouds. The horizontal axis label is modeled grid points. The vertical axis label is height in km.

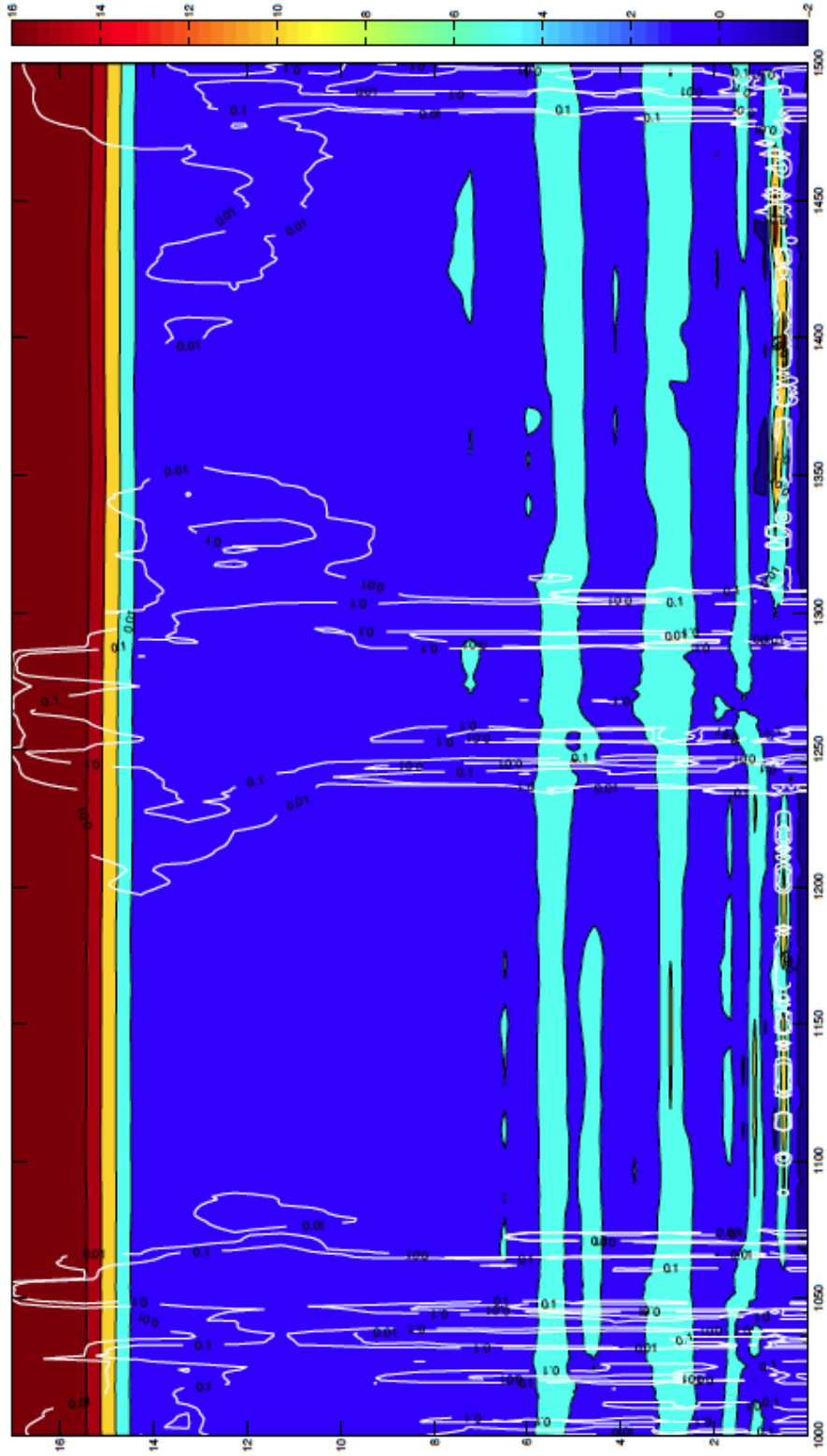


**Figure 14:** Filled contours are potential temperature lapse rate. Open contours are maximum value of total condensate mixing ratio along the meridional direction - they outline clouds. The horizontal axis label is modeled grid points. The vertical axis label is height in km.

Disturbed regions can be seen as the regions of deep, high values of total condensate; the undisturbed regions can be seen as regions of higher stability and low-level cloudiness. The overall size of the undisturbed region shrinks in SST302 as has been shown above. Also, the stratosphere, here characterized by the upper levels of strong stability, moves vertically as has been seen above. The split stable layers of the boundary layer decrease in magnitude dramatically. In SST298, the peak stability is about  $20 \text{ K km}^{-1}$  while in SST302, it is only  $16 \text{ K km}^{-1}$  and much less spatially extensive. Above this, the stable layer associated with the freezing level is both split and very weak in SST302. Between the stable layers, the air is much less stable in SST302 than SST298. The SST302 profile shows a lapse rate of nearly  $0 \text{ K km}^{-1}$  everywhere between the stable layers. Though not shown because it's difficult to quantify, the subsiding winds in SST302 can be much weaker than in SST298.

Pakula *et al* (2009) introduced a method by which the contributions of radiation to the modeled stable regions can be assessed. This method indirectly allows for the assessment of the dynamical contributions as well. The technique shows that radiation contributes only a few  $\text{K day}^{-1}$  ( $\sim 4$ ) to the modeled stable layers. It contributes more in SST298 than in SST302 by a factor of  $\sim 2$  probably because of the greater vertical RH gradients in the cooler model run. The small contribution by radiative effects to the stability implies, as Pakula *et al* found in their study, they are insignificant compared to the dynamical contributions. The dynamical effects are taken here to include the thermodynamic effects since there is no way to assess them independently without clouds to imply local latent heating. Taken together, these contributions must decrease,

given the large decrease in stability with SST even with the decrease in contributions from radiation.

The subsidence above the freezing level is driven by the diabatic convergence in the UT. In the last chapter, it was shown to decrease with SST. The previous section explained that the dynamic contributions to stability decrease. These both would imply a lessened domain mean circulation subsidence above the freezing level. This makes the stable layers less stable. If these stable layers are weaker, the circulations below that level are less confined to the lower levels. These circulations, therefore, could decrease significantly. More quiescent flow in the super freezing, undisturbed regions could feed back to the disturbed region circulations through the direct ingestion, at those levels, of the less stable air.

## VIII: CLOUD TOP CHANGES

It has been shown in the previous few chapters that the circulation changes in the disturbed and undisturbed regions act to reinforce one another. This feedback loop has obvious implications for the state of convection. The less obvious are those effects on climate. The potential climatic impacts of the tropical atmosphere could be the result of the WV concentration, since these affect LW emission from undisturbed regions, and cloud distributions and properties, since these affect LW emission from cloud top and SW reflection. Perhaps leading to some sense of the types of climate impacts to be discussed below was the earlier mention of a variety of anvil feedbacks: the FAT, Thermostat, and Iris Hypotheses. Each will be examined here as components of a single feedback. To the best of the author's knowledge, these anvil feedbacks have never been discussed together.

Unlike what the FAT would suggest, anvils here are seen to detrain at colder temperatures with warmer SSTs – an unambiguously positive climate feedback. The cloud top temperature sensitivity of  $-1\text{K K}^{-1}$  would reduce OLR in disturbed regions by about  $2.0\text{ W m}^{-2}\text{ K}^{-1}$ . The crucial ingredient in the model which would imply such a sensitivity converse to the FAT is the increase in UT RH with SST. It was shown in Chapter V that an increase in UT RH shifts the detrainment level to colder temperatures.

Much can also be made of the decreased sharpness in the detrainment peak as shown in Figure 13. It was noted earlier that cloud top temperatures are more variable in SST302, and Figure 12 would seem to suggest why. The wider detrainment maximum in pressure space may also hint at how anvils shapes could change. The broader peak could, in principle, detrain clouds that are physically thicker. If the ice concentration and properties of anvil clouds are assumed to remain constant, then physically thicker clouds are optically thicker ones. Thicker anvils are predicted by the Thermostat Hypothesis. Some analysis of SW up at TOA above regions identified as having high clouds indicates that total SW reflected by anvils increases by  $2.0 \text{ W m}^{-2} \text{ K}^{-1}$  in SST302. The LW effect is negligible due to the thinness of the LW skin depth of clouds.

There is some circumstantial evidence to support both of these claims. It would be difficult to show here, but through visual examination of modeled cloud fields, anvils do appear to get thicker and move to colder temperatures in many of the scenes. Mathematically, unambiguously identifying anvils without getting contamination from convective cores or convective areas within anvils can prove difficult so creating statistics to show anvil thickness is not done here.

The occurrence of an iris in the model is difficult to prove; however much data can be suggestive of such a climate feedback especially given its place with the other two anvil feedbacks above. As above, the issue with examining the Iris feedback is identifying mathematically areas of anvil clouds, convective cores, and separating independent areas. Defining each is also an issue. To remain terse, only a single mathematical definition of core and anvil will be used. Anvils have been defined using

an OLR threshold of  $125 \text{ W m}^{-2}$ . Convective cores have been defined using a  $6 \text{ mm hr}^{-1}$  rain rate threshold. These thresholds were taken to be well representative. Various other definitions used, but not shown here, involve a total condensate threshold for ice above 8 km for anvils, and vertical velocity for cores as well as various magnitudes of all thresholds. Trends are insensitive to the precise definition used, but the magnitudes are. As such, only the types of changes will be emphasized.

The unavoidable issue with using the definitions above to examine the iris is that cloud anvils tend to overlap and coincide with one another in the disturbed regions. So while it would be ideal to calculate just how much anvil each core contributes to the UT, this is impossible. Therefore, the first number to assess is how much total anvil cloud area exists in the last week of the simulation divided by the total number of convective cores. This yields  $1,053 \text{ km}^2$  per core in SST298 and  $969 \text{ km}^2$  per core in SST302. This is a decrease of  $2\% \text{ K}^{-1}$ . However, these numbers include many overlapping anvils. To get a sense for the overlap, the number of cores per contiguous anvil region analyzed by the computer can be calculated. There are 1.30 cores per anvil region in SST298 and 1.47 in SST302. The increase indicates an increase in the likelihood of an anvil region covering multiple cores. The size of isolated anvils per core is  $10,084 \text{ km}^2$  in SST298 and  $8,108 \text{ km}^2$  in SST302. Each of these numbers is indicative of an iris type feedback.

The combination of all three of these cloud feedbacks provides a good picture for how, and why, anvils change the way they do given the circulation feedback discussed previously. The DC maximum in the UT broadens, weakens, and rises with SST. This combination leads to anvils that are higher and cooler as well as thicker. Though the

convective mass flux decreases, the amount of cloud ice at the upper levels increases slightly with SST but by less than the anvils thicken. Because the clouds are physically thicker, they are also less spatially extensive if their ice concentrations remain nearly fixed. Posselt *et al* (*In Press*) actually even show that ice path actually increases in the UT. The combined feedback needs a name: the CAT-eye-ostat or CAT-ostat-iris, perhaps.

## IX: Synthesis

The previous chapters tried to build a coherent picture of a convective circulation feedback and its effects on cloud tops that appears to be strongly modulated by SSTs. It was argued that many of the components made basic physical sense and may, at this point, seem to have been assumed from the beginning. The not so obvious answer is to why, from a system wide perspective, does this feedback make sense. What does the atmosphere gain from being in this new state?

First, it will be noted that Figure 15 shows in a cartoon the entire circulation and cloud top feedback developed here. The trends in the figure are in relation to increasing SSTs and represent the mean atmosphere. It can be seen that both the circulation and radiative processes, act in concert to destabilize and stabilize the atmosphere in SST302 as compared to SST298 in such a way that each component of the circulation allows for the existence of another. The increased height of the tropopause acts to stabilize through its effects on potential temperature. The lessened distance between disturbed regions and weaker stable layers is a response to the destabilization. Finally, the increasing UT RH may be understood as either a driving mechanism or an ultimate response.

Many have previously modeled atmospheric circulations as heat engines. Perhaps the most widely seen example is from Emanuel in 1986. While never a perfect

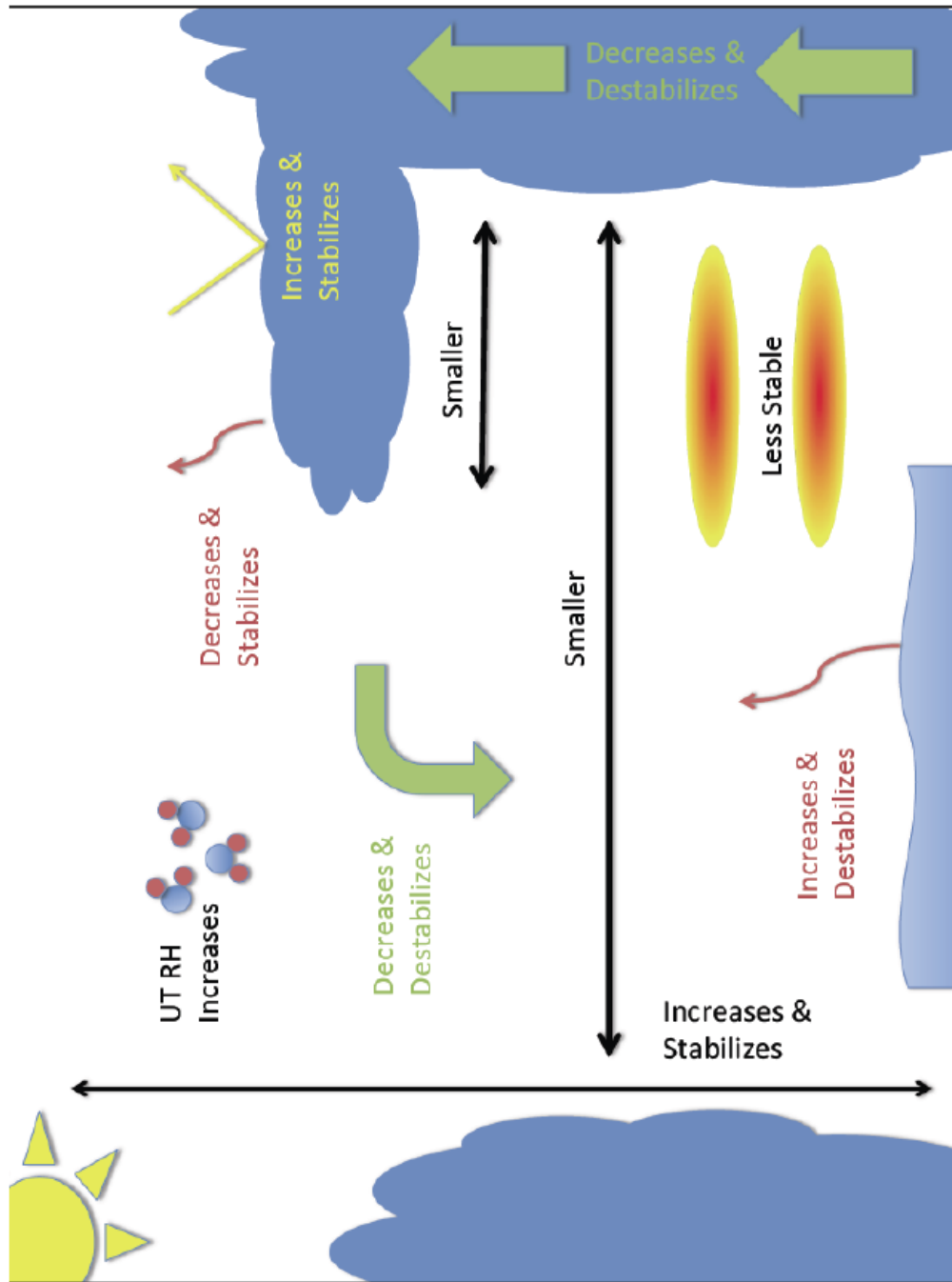


**Figure 15:** A cartoon diagram of the proposed components of the convective feedback system. On the left and right are clouds. Green arrows show air circulations. Red lines are thermal emission. Black lines are distances. The yellow line is solar radiation. The orange ovals are meant to represent undisturbed region stable layers. Finally the cartoon blue and red circles are water vapor molecules.

analogy, the paradigm has proven useful in understanding how energy is used in the atmosphere to drive certain processes. In that spirit, Figure 16 shows how the convective circulation might be understood. A saturated air parcel with surface

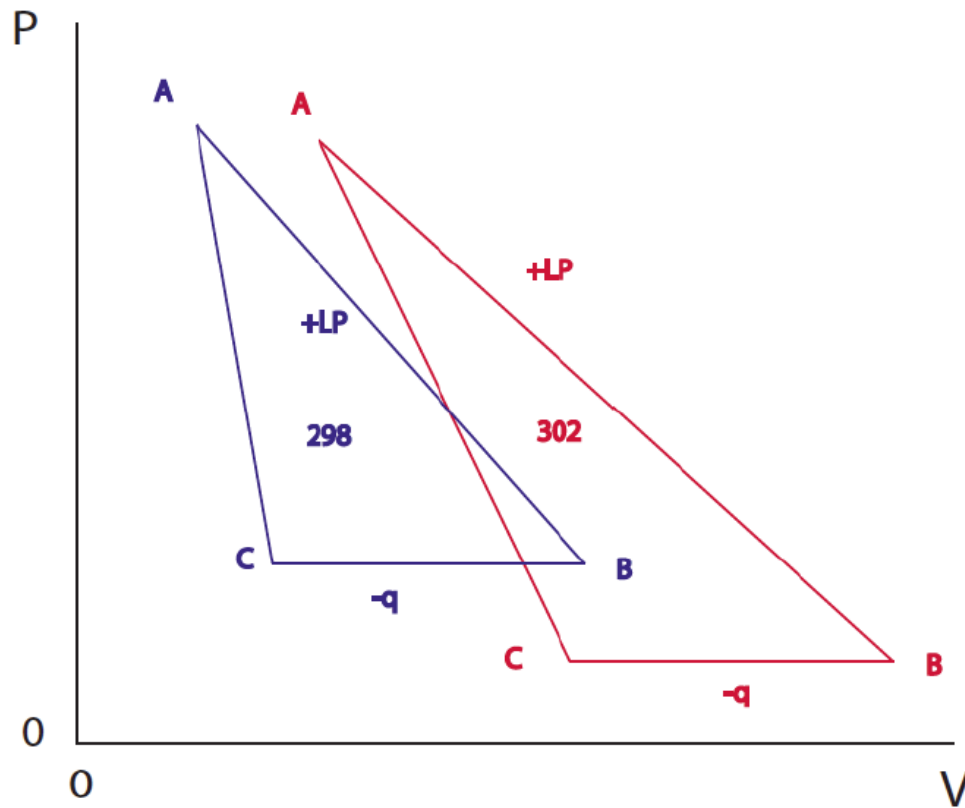


**Figure 16:** A theoretical PV diagram of the convective heat engine. 298 is in blue, and 302 is in red. Local adiabats are quasi-parallel to the lines from C to A. A to B is pseudo-adiabatic expansion along ascent into clouds. Latent heat equal to  $L \cdot P$  is released. B to C is isobaric compression. Clouds cool to space equal to  $-q$ . C to A is adiabatic compression.

pressure (P) begins its ascent into a convective cell at point A. It rises pseudoadiabatically to cloud top at point B. From there it detrains at nearly constant pressure and cools which lessens the parcel volume (V). After detraining to point C, the parcel subsides in the undisturbed region adiabatically back to point A. The work done in a heat engine is the integrated area inside the curve. Point A in 302 is slightly warmer (more V), but at nearly the same P as 298. 302, however, is able to access much lower pressure from B to C than is 298. In its ability to do so, it adds much more area to

the inside of the PV curve. While in 302 the parcel cools less from B to C, it is at a lower pressure so the change in volume along this leg remains nearly constant. This implies more work is done per cycle in 302 than 298. While many important processes are disregarded in this model, it nonetheless sheds some light on why the new state is desirable to the system.

This cycle is not without a mechanical analogue. Legs B to C and C to A are reminiscent of the isobaric and isentropic compression legs in a Brayton engine. And in some ways, leg A to B is similar to the expansion legs of the Brayton cycle. If all the energy released by vapor condensation were done so at the surface and the parcel allowed to expand in response to its new temperature and then allowed to rise adiabatically to its level of neutral buoyancy, the cycle proposed above would be precisely a Brayton cycle. A mechanical analogue is important to show that such a cycle actually produces a desired outcome: work.

The efficiency of any heat engine can be defined as 1 minus the exhaust energy over the input energy. That results is:

$$E = \frac{\textit{benefit}}{\textit{input}} = \frac{Q_H - Q_C}{Q_H} = 1 - \frac{Q_C}{Q_H} \quad (\text{EQ 17})$$

where Q is some amount of heat. Subscripts mean hot (H) and cold (C). For the heat engine designed in this chapter,  $Q_C$  may be thought of as the cooling to space,  $\dot{q}$ , by the cloud top (an exhaust of heat), and the input,  $Q_H$ , could be condensational heating of the parcel,  $L^*Prec$ . All of these are average parcels. The ratio of efficiencies from 302 to 298, then becomes:

$$\frac{E_{302}}{E_{298}} = \frac{1 - \frac{\dot{q}_{302}}{L * Pr_{302}}}{1 - \frac{\dot{q}_{298}}{L * Pr_{298}}} \text{ (EQ 18).}$$

If  $\alpha$  is the ratio of cloud top cooling in 298 to 302 and  $\beta$  that of latent heating in 302 to 298, then both are greater than one. Thus the ratio of efficiencies may be easily seen to be greater than unity when in the form:

$$\frac{E_{302}}{E_{298}} = \frac{1 - \frac{\dot{q}}{\beta L * Pr}}{1 - \frac{\alpha \dot{q}}{L * Pr}} = \frac{\beta L * Pr - \dot{q}}{L * Pr - \alpha \dot{q}} \text{ (EQ 19).}$$

Using this simple model, the efficiency ratio of the convective state of SST302 over SST298 is 1.22. The ratio's being greater than unity implies an increased efficiency. Noting this is an important result. A greater efficiency could imply that the atmosphere is now in a more "preferred" state. If that is the case, then the SST does not serve to force the new atmospheric setup but simply allows the atmosphere to enter it. If it can be assumed that the atmosphere will always adjust into the most efficient possible state accessible to it, then a wide variety of non-linear responses, such as those listed above, to what have traditionally been thought of as a "forcing" may be possible.

### *Entropy*

In an ideal Brayton cycle, the maximum efficiency is achieved with the greatest possible ratio of the input and output temperatures. In the context of the heat engine developed here, that means efficiency is maximized in 302 with respect to 298 with more latent heating (greater  $\beta$ ) and less thermal cooling (greater  $\alpha$ ). Both of those criteria also imply a greater entropy production. More latent heating means greater

expansion from A to B and consequently more entropy production. Since the change in entropy from B to C is the ratio of the thermal emission rate to the temperature, if as a percent, temperature changes more than emission, more entropy will be produced in 302. These ideas fit well with the theory of maximum entropy production that posits that a variety of non-equilibrium thermodynamic systems adjust into a state such that the production of entropy is maximized (Paltridge, 1978; Dewar 2003). Approximately calculated, the rate of entropy production increases from 298 to 302 by a factor of 1.5. A more detailed description than this is beyond the scope of what I would like to show here, but should be done in the future.

### *Precipitation*

It was mentioned in chapter III that the characteristics of precipitation change with SST as does the overall amount. The explanation for the total accumulated rainfall change lies in the enhanced evaporation of the warmer atmospheric state. The reasons for the enumerated changes in the intensity were not given at the time, as they needed to be built. Now, the previous chapters have helped to paint a picture as to why, perhaps, the rain rates changes in the way they do.

While the convective mass flux diagram (Figure 4) clearly shows a decrease in convective intensity with SST, it does so only in the average. Individual storms should actually be more intense in the warmer state because the extra latent heating provided by the increased moisture availability should enhance updrafts. This could be true even given the decreased  $M_C$  if the convective area decrease were more than the decrease in

convective flux. Indeed convective updrafts increase within disturbed regions especially in the middle troposphere (not shown, but easily understood from Figure 4).

If the efficiency of the heat engine proposed just above is calculated in the standard way as a ratio of pressures, the increased engine efficiency can be understood not as being driven by the precipitation, but as producing it. Since the logic is circular it makes no difference in which way the engine is imagined. In this manner of thinking, the change in pressure can be supposed to “wring out” water vapor in the form of rain. Since in SST302 there is an increased variability in cloud top pressure (see chapter IV), there is also an increased variability in how much water is “wrung out” of the column. Taken together, the increased compression ratio and variability may hint at the change in the intensity and distribution of rain rates. This method of thinking is only relevant to rain, not drizzle since drizzle is often controlled by more local thermodynamic and microphysical properties of clouds.

## X: OBSERVATIONAL EVIDENCE

Up to this point, the results have been derived from a variety of models. While models are an excellent platform in which to develop theories, it is crucial to test whether these theories hold up to observational testing. To that end, and to the extent that certain aspects of the above feedbacks are observable without *in situ* observations tailored to their elucidation, CloudSat and CALIPSO will help shed some light on the real world magnitudes of the cloud-climate relations.

CloudSat and CALIPSO provide complimentary data in the UT. The combined cloud product, is therefore, used to measure anvil activity. Cloud tops are taken to be the first pixel from the top with a positive identification of clouds in the GEOPROF-lidar product. Cloud tops, obviously, do not correspond to peak cloud frequency. They are presented here because the data is very clean as the attenuation algorithms have not yet degraded the data and because the same conclusions will be drawn about the nature of observed anvil clouds. The average DC profile is calculated from the mean of 3 million tropical profiles. It uses environmental variables provided by ECMWF reanalysis and flux-heating rate product. Each profile is passed through a moving average, low pass filter. Smoothing is necessary as the DC calculation requires a derivative of a derivative which provides some numerical noise. The filtering takes out the high frequency noise but also damps the magnitude of the result. As such, DC is

underestimated. Also, to fall in line with the modeled atmospheres of SST298 and SST302, only ocean pixels are used. Data are screened to be tropical only (30°S-30°N). Finally, satellite granules were chosen randomly so as not to bias potentially the results to any climate state.

Next, the DC profiles were binned by ECMWF SST. The SST bins are 297K-299.5K, the 298K bin, and 300.5K-303K, the 302K bin. The bins are wide to capture more of the available data. Each bin is not centered on its respective nominal temperature. This has been done at the low end to prevent contamination from SSTs too low to be consistently convective, and on the high end to avoid the theorized convective state transition at 30°C. Figure 17 shows the dependence of the DC results of SST. There is a change in the color scheme in this plot to indicate it does not use model data. The observed DC maximum occurs at 209K in 298K. The maximum cools in 302K to 206K. These numbers are impressively similar to the modeled results. The sensitivity, though, is less. Not only does the temperature of the observed DC maximum decrease with SST, but also the peak widens as in the simulations.

Figure 18 shows the general agreement between the DC maximum and the cloud top distribution peak. The cloud top distribution peaks slightly higher than does DC from each respective bin of Figure 16. This is to be expected as the results showing cloud top should slightly overlay the cloud maximum. The agreement provides some suggestive evidence that the assumption that DC controls anvil detrainment is at least somewhat valid. Correlation, though, is not causation. Nonetheless, cloud top temperature does robustly appear to decrease with SST. The cloud percentage has been normalized as in Kuang and Hartmann (2008) to ease comparison.

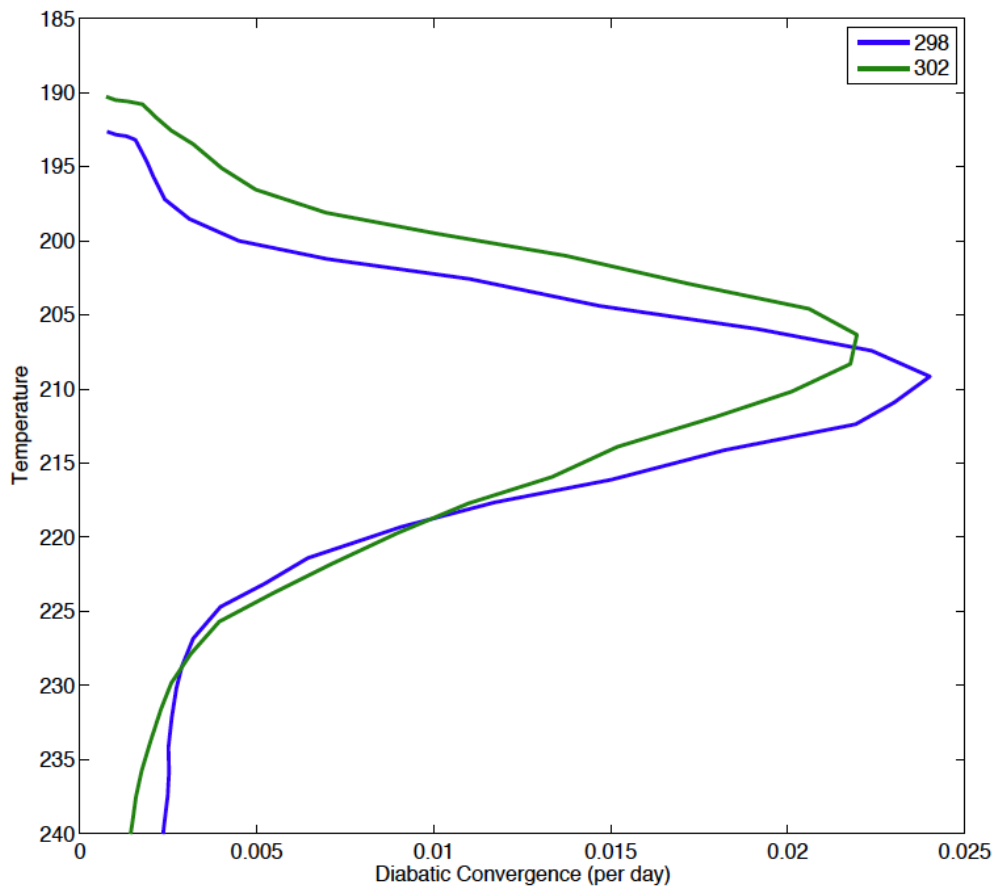


**Figure 17:** Observed diabatic convergence. The data is binned by sea surface temperature. Data from the 298K bin is in blue, and data from the 302K bin is in green.

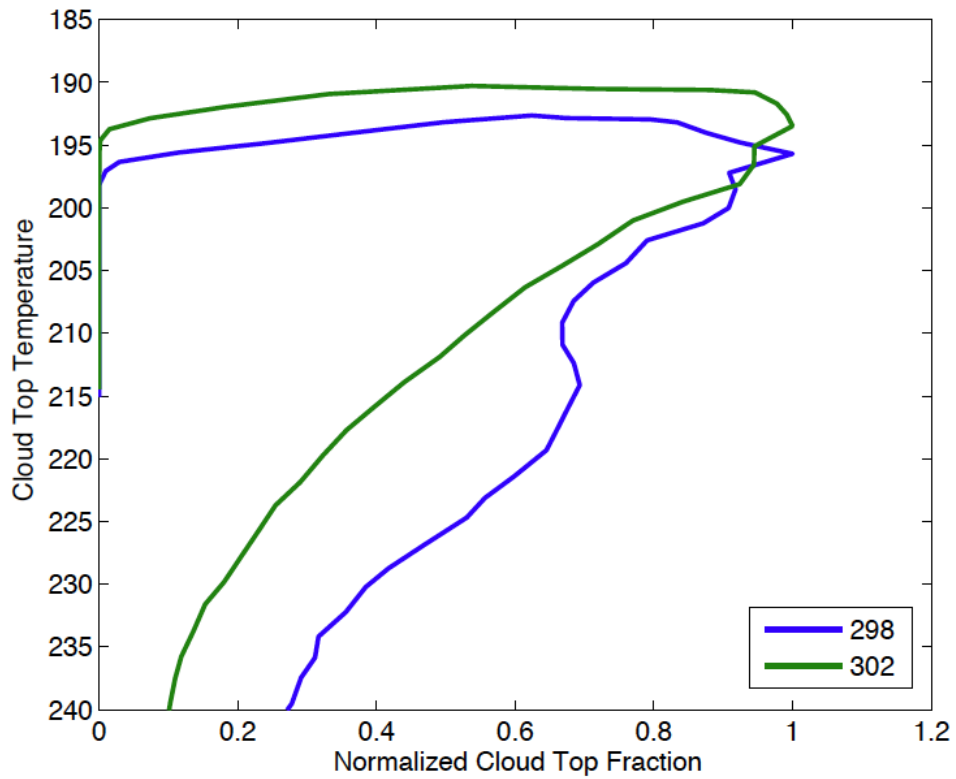


**Figure 18:** Observed cloud top height temperatures. Data binned to a sea surface temperature of 298 K is in blue, and data binned to 302 K is in green.

## XI: SUMMARY AND CONCLUSIONS

The tropical convective atmosphere has received increased attention as atmospheric science has shifted from solving mid-latitude, daily weather problems to issues affecting climate. It has come to be understood that the state of the tropical atmosphere has profound effects, through tele-connections, radiation, or the general circulation, on the state of the atmosphere over the rest of the globe. The convective circulation and convective anvil feedback modulated by SST described above seeks to add a valuable piece to building our understanding of the tropical atmosphere. The study was a simple one. One that assumed the modulation depended solely on SST. From that basic assumption, the results were drawn.

It has been found that UT RH increases with increasing SST. Using the water budget fluxes into and out of the disturbed and undisturbed regions into which the model organizes its convection, the RH increase was understood to result from the shifting nature, controlled by the basic model physics, of the components of the flux. Elsewhere it has been understood by looking at the intensity of the general circulation. Precipitation was seen to increase at a rate slower than the CC rate would seem to imply, and that intense convection increased at the expense of the weak. The convective fluxes reflected these findings as it decreased with SST. The stability and vertical structure of undisturbed regions change such that the increase in instability

may help to prime convection in the disturbed regions. These domain mean type findings were used to show that the nature of convection was changing with SST. The rest of the analysis was done to show why such changes occur.

The dependences in the UT on RH were derived from basic radiation principles. It was found that the ability of the atmosphere to effectively cool via LW to space depends on RH. An assessment found that a 10% increase in UT RH decreased temperature of the cooling maximum by 2.4K. The sensitivity of the cooling rate to RH was assessed mathematically for the first time. A BugsRad assessment seemed to confirm the sensitivity to RH. Since the cooling maximum dictates the level and temperature of detraining anvil clouds, it was theorized that the temperature of anvils, and therefore the amount of thermal emission from their surface would also decrease. This dependence was then checked in the modeled atmosphere. The LW cooling profiles were seen to change in pressure space, as a result of the deepening of the troposphere with SST, and change in magnitude. The variation in the LW profiles implied different diabatic heating profiles in the UT of the two, modeled states. As the FAT hypothesis theorized, most of the DC profile is controlled entirely by temperature, in the UT, though, the SST298 and SST302 profiles diverged and the warmer SST simulation peaked at a lower temperature just like the simple thought experiment model. Finally, an attempt was made to show that these diverse elements work in concert in the atmosphere to form a new, preferred state that seeks to maximize potential efficiency and entropy production in-line with theory.

There are several aspects of this study which due to current computer resources or observational limitations are not ideal. First, the vertical spacing in the upper

troposphere is on the order of a kilometer. This limits the ability of the model to resolve anvil structure, and in some instances, decreases their horizontal extent due to artificially, vertically distributing condensate concentrations. Second, the cloud microphysical scheme is rudimentary. A more advanced scheme could help to model better ice processes. Cloudsat and CALIPSO provide an unparalleled ability to map cirrus, but many of the arguments below are based on clear sky heating. This analysis relied on reanalysis projections of heating rates in the UT. A direct measurement would have been useful. Noting that both the model and observations could stand to be improved, there is certainly more work that could be done to understand these systems.

Finally, some effort has been made above to frame the importance of this feedback, but more can be made of its potential importance. If indeed the LW and SW components of the anvil radiative feedback do cancel in reality, as here, the role of clouds in the climate response system could remain muddled. If the LW component is a part of the destabilization feedback of the tropical convective system and the SW a response, there may yet be some room for an overall negative forcing. The importance of understanding the forcing due to tropical convective systems should not be underestimated. Also, a better understanding of the ways in which different aspects of the tropical convective circulation interact is crucial to a wide range of meteorologically important physics not the least of which is its role in the general circulation. Convective circulation feedbacks may also be important to understanding phenomena such as the Madden-Julian Oscillation that meter precipitation.

## WORKS CITED

- Allen, M. R., and W. J. Ingram, 2002: Constraints on future changes in climate and the hydrologic cycle. *Nature*, **419**, 224-228.
- Dewar, R., 2003: Information theory explanation of the fluctuation theorem, maximum entropy production and self-organized criticality in non-equilibrium stationary states. *Journal of Physics A: Mathematical and General*, **36**, 631-641.
- Emanuel, K. A., 1986: An Air-Sea Interaction Theory for Tropical Cyclones. Part-I: Steady State Maintenance. *Journal of the Atmospheric Sciences*, **43**, 585-604.
- Fitzjarrald, D. R., M. Garstang, 1981: Vertical Structure of the Tropical Boundary Layer. *Mon. Wea. Rev.*, **109**, 1512-1526.
- Fu, R., A. D. Del Genio, W. B. Rossow, and W T Liu, 1992: Cirrus-cloud thermostat for tropical sea surface temperatures tested using satellite data. *Nature*, **358**, doi:10.1038/358394a0
- Fu, Q., and K-N. Liou, 1992: On the correlated k-distribution method for radiative transfer in nonhomogenous atmospheres. *Journal of the Atmospheric Sciences*, **49**, 2139-2156.
- Grabowski, W. W., and M. W. Moncrief, 2001: Large-scale organization of tropical convection in two-dimensional explicit numerical simulations. *Quarterly Journal of the Royal Meteorological Society*, **127**, 445-468.
- Larson, K. and D. L. Hartmann, 2003: Interactions among Cloud, Water Vapor, Radiation, and Large-Scale Circulation in the Tropical Climate. Part I: Sensitivity to Uniform Sea Surface Temperature Changes. *Journal of Climate*, **16**, 1425-1440.
- Lau, K. M., C. H. Sui, and W. K. Tao, 1993: A Preliminary Study Of The Tropical Water Cycle And Its Sensitivity To Surface Warming. *Bulletin of the American Meteorological Society*, **74**, 1313-1321.
- L'Ecuyer, T., D. Vane, G. Stephens, and D. Reinke, 2007: Level 2 Fluxes and Heating Rate Product: Process Description and Interface Control Document. Cloudsat Data Processing Center.
- Lindzen, R. S., M. D. Chou, and A. Y. Hou, 2001: Does the earth have an adaptive infrared iris? *Bulletin of the American Meteorological Society*, **82**, 417-432.
- Harries, J. E., 1996: The greenhouse Earth: A view from space. *Quarterly Journal of the Royal Meteorological Society*, **122**, 799-818.
- Harrington, J. Y., 1997: The effects of radiative and microphysical processes on simulated warm and transition season Arctic stratus. Ph.D dissertation, Colorado State University, 289 pp.
- Hartmann, D. L., L. A. Moy, and Q. Fu, 2001: Tropical Convection and the Energy Balance at the Top of the Atmosphere. *Journal of Climate*, **14**, 4495-4511.

- van den Heever, S. C., and coauthors, 2011: Mesoscale Circulations in a Modeled, Convective Atmosphere. *Submitted*.
- Held, I. M. and B. J. Soden, 2006: Robust Responses of the Hydrological Cycle to Global Warming. *Journal of Climate*, **19**, 5686-5699.
- Highwood, E. J. and B. J. Hoskins, 1998: The tropical tropopause. *Quarterly Journal of the Royal Meteorological Society*, **124**, 1579-1604.
- Hill, G. E., 1974: Factors controlling the size and spacing of cumulus clouds as revealed by numerical experiments. *Journal of the Atmospheric Sciences*, **31**, 646.
- Ingram, W. J., 2002: On the Robustness of the Water Vapor Feedback: GCM Vertical Resolution and Formulation. *Journal of Climate*, **15**, 917-921.
- Jensen, E. J., O. B. Toon, H. B. Selkirk, J. D. Spinhirne, and M. R. Schoeberl, 1996: One the formation and persistence of subvisible cirrus clouds near the tropical tropopause. *Journal of Geophysical Research*, **101**, 21,361-21,375.
- Johnson, R. H., T. M. Rickenbach, S. A. Rutledge, P. E. Ciesielski, and W. H. Schubert, 1999: Trimodal characteristics of tropical convection. *Journal of Climate*, **12**, 2397-2418.
- Kuang, Z. and D. L. Hartmann, 2007: Testing the Fixed Anvil Temperature Hypothesis in a Cloud-Resolving Model. *Journal of Climate*, **20**, 2051-2057.
- Lilly, D. K., 1962: On the numerical simulation of buoyant convection. *Tellus*, **XIV**, 148-172.
- Mace, G., D. Vane, G. Stephens, and D. Rieneke, 2007: Level 2 Radar-Lidar GEOPROF Product Version 1.0: Process Description and Interface Control Document. Cloudsat Data Processing Center.
- Manabe, S. and R. F. Strickler, 1964: Thermal Equilibrium of the Atmosphere with a Convective Adjustment. *Journal of the Atmospheric Sciences*, **21**, 361-385.
- Mapes, B. E., 1993: Gregarious Tropical Convection, *Journal of the Atmospheric Sciences*, **50**, 2026-2037.
- Mapes, B. E. and R. A. Houze, 1995: Diabatic Divergence Profiles in Western Pacific Mesoscale Convective Systems. *Journal of the Atmospheric Sciences*, **52**, 1807-1828.
- Muller, C. J. and P. A. O’Gorman, 2011: Intensification of Precipitation Extremes with Warming in a Cloud-Resolving Model. *Journal of Climate*, **24**, 2784-2800.
- Pakula, L. and G. L. Stephens, 2009: The Role in Influencing Tropical Cloud Distributions in a Radiative-Covective Equilibrium Cloud-Resolving Model. *Journal of the Atmospheric Sciences*, **66**, DOI: 10.1175/2008JAS2738.1.
- Paltridge, G. W., 1978: The steady-state format of global climate. *Quarterly Journal of the Royal Meteorological Society*, **104**, 927-945.
- Pierrehumbert, R., 1995: Thermostats, radiator fins, and the local runaway greenhouse. *Journal of the Atmospheric Sciences*, **52**, 241-259.
- Pielki, R. A., and coauthors, 1992: A Comprehensive Meteorological Modeling System – RAMS. *Meteorology and Atmospheric Physics*, **49**, 69-91.
- Posselt, D. J., S. C. van den Heever, and G. L. Stephens, 2008: Trimodal cloudiness and tropical stable layers in simulations of radiative convective equilibrium. *Geophysical Research Letters*, **35**, doi: 10.1029/2007GL033029.

- Posselt, D. J., S. C. van den Heever, G. L. Stephens, and M. R. Igel, 2011: Changes in the interaction between tropical convection, radiation and the large scale circulation in a warming environment. *Journal of Climate*, *Submitted*.
- Ramanathan, V. and W. Collins, 1991: Thermodynamic regulation of ocean warming by cirrus clouds deduced from observations of the 1987 El Nino. *Nature*, **351**, 27-32.
- Robe, F. R. and K. A. Emanuel, 1996: Moist convective scaling: some inferences from three-dimensional cloud simulations. *Journal of the Atmospheric Sciences*, **53**, 3265-3275.
- Ryoo, J.-M., T. Igusa, and D. W. Waugh, 2009: PDFs of Tropical Tropospheric Humidity: Measurements and Theory. *Journal of Climate*, **22**, DOI: 10.1175/2008JCLI2747.1.
- Salby, M. L., 1996: *Fundamentals of Atmospheric Physics*. Academic Press, 627.
- Sherwood, S. C., W. Ingram, Y. Tsushima, M. Satoh, M. Roberts, P. L. Vidale, and P. A. O’Gorman (2010), Relative humidity changes in a warmer climate, *J. Geophys. Res.*, 115, D09104, doi:10.1029/2009JD012585.
- Smagorinsky, J., 1963: General circulation experiments with the primitive equations. Part I, The basic experiment. *Monthly Weather Review*, **91**, 99-164.
- Soden, B. J., and F. P. Bretherton, 1993: Upper tropospheric relative humidity from the GOES 6.7  $\mu\text{m}$  channel: Method and climatology for July 1987. *Journal of Geophysical Research*, **98**, 16,669-16,688.
- Stephens, G. L., S.-C. Tsay, P. W. Stackhouse, P. J. Flatau, 1990a: The Relevance of the Microphysical and Radiative Properties of Cirrus Clouds to Climate and Climatic Feedback. *J. Atmos. Sci.*, **47**, 1742–1754.
- Stephens, G. L., 1990b: On the Relationship between Water Vapor Over the Oceans and Sea Surface Temperatures. *Journal of Climate*, **3**, 634-645.
- Stephens, G. L., D. L. Jackson, and I. Wittmeyer, 1996: Global Observations of Upper Tropospheric Water Vapor Derived from TOVS Radiance Data. *Journal of Climate*, **9**, 305-326.
- Stephens, G. L., P. M. Gabriel, and P. T. Partain, 2001: Parameterization of atmospheric radiative transfer, Part I: Validity of simple models. *Journal of the Atmospheric Sciences*, **58**, 3391-3409.
- Stephens, G. L. and D. G. Vane, 2007: Cloud Remote Sensing in the era of the A-Train. *Journal of Applied Remote Sensing*, **1**, 013507.
- Stephens, G. L., S. van den Heever, and L. Pakula, 2008a: Radiative-Convective Feedbacks in Idealized States of Radiative-Convective Equilibrium. *Journal of the Atmospheric Sciences*, **65**, 3899-3916.
- Stephens, G. L. and T. D. Ellis, 2008b: Controls of Global Mean Precipitation Increases in Global Warming GCM Experiments. *Journal of Climate*, **21**, 6141-6155.
- Stephens, G. L. and Y. X. Hu, 2010: Are climate-related changes to the character of global-mean precipitation predictable? *Environmental Research Letters*, **5**, doi: 10.1088/1748-9326/5/2/025209.

- Su, H., C. S. Bretherton, and S. S. Chen, 2000: Self-Aggregation and Large Scale Control of Tropical Deep Convection: A Modeling Study. *Journal of the Atmospheric Sciences*, **57**, 1797-1816.
- Su, H., and coauthors, 2008: Variations of tropical upper tropospheric clouds with sea surface temperature and implications for radiative effects. *Journal of Geophysical Research*, **113**, doi:10.1029/2007JD009624.
- Tompkins, A. M., 2000: The Impact of Dimensionality on Long-Term Cloud-Resolving Model Simulations. *Monthly Weather Review*, **128**, 1521-1535.
- Tompkins, A. M., 2001: Organization of Tropical Convection in Low Vertical Wind Shears: The Role of Water Vapor. *Journal of the Atmospheric Sciences*, **58**, 529-545.
- Trenberth, K. E., J. Fasullo, and L. Smith, 2005: Trends and variability in column-integrated atmospheric water vapor. *Climate Dynamics*, **24**, 741-758.
- Tripoli, G. J. and W. R. Cotton, 1982: The Colorado State University three-dimensional cloud/mesoscale model – 1982. Part I: General theoretical framework and sensitivity experiments. *Journal of Atmospheric Research*, **16**, 185-220.
- Vecchi, G. A. and B. J. Soden, 2007: Global Warming and the Tropical Circulation. *Journal of Climate*, **20**, 4316-4340.
- Walko, R. L. and Coauthors, 2000: Coupled atmosphere-biophysics-hydrology models for environmental modeling. *Journal of Applied Meteorology*, **39**, 931-944.
- Wentz, F. J., L. Ricciardulli, K. Hilburn, and C. Mears, 2007: How much more rain will global warming bring? *Science*, **317**, 233-235.
- Ye B., A. D. Del Genio, and K. W.-L. Lo, 1998: CAPE Variations in the Current Climate and Climate Change. *Journal of Climate*, **11**, 1997-2015.
- Zelinka, M. D. and D. L. Hartmann, 2010: Why is the longwave cloud feedback positive? *Journal of Geophysical Research*, **115**, doi:10.1029/2010JD013817.